Simultaneous Positioning and Orientating (SPAO) for Visible Light Communications: Algorithm Design and Performance Analysis

Bingpeng Zhou[†‡], Vincent Lau[‡], Qingchun Chen[♯] and Yue Cao[⋆]
[†]Shenzhen Research Institute, Hong Kong University of Science and Technology, Shenzhen, China.
[‡]Dept. of ECE, Hong Kong University of Science and Technology, Hong Kong 999077, China
[♯]Guangzhou University, Guangzhou, Guangdong 510006, China
[⋆]Northumbria University, Newcastle NE1 8ST, UK
eebzhou@ust.hk, eeknlau@ee.ust.hk, qcchen@gzhu.edu.cn, yue.cao@northumbria.ac.uk

***Abstract*—Visible light communication (VLC)-based simultaneous positioning and orientating (SPAO), using received signal strength (RSS) measurements, is studied in this paper. RSS-based SPAO for VLCs of great challenge as it is essentially a non-convex optimization problem due to the nonlinear RSS model. To address this non-convexity challenge, a novel particle-assisted stochastic search (PASS) algorithm is proposed. The proposed PASS-based SPAO scheme does not require the knowledge of the height of receiver, the perfect alignment of transceiver orientations or inertial measurements. This is a huge technical improvement over the existing VLC localization solutions. The algorithmic convergence is established to justify the proposed PASS algorithm. In addition, a closed-form Cramer-Rao lower bound (CRLB) on localization error is derived and analyzed to gain insights into how the VLC-based SPAO performance is related to system configurations. It is shown that the receiver's position and orientation accuracy is linear with signal-to-noise ratio and direction information. In addition, the position accuracy decays with six powers of the transceiver distance, while the orientation accuracy decays with four powers of the transceiver distance. Finally, simulation results verify the performance gain of the proposed PASS algorithm for VLC-based SPAO.**

***Index Terms*—Visible light communication, positioning and orientating, non-convex optimization, PSO, Cramer-Rao bound.**

I. Introduction

VISIBLE light communication (VLC)-based localization has attracted increasing research attentions recently [1], [2], [3], along with emerging VLC techniques [4]. VLC-based localization would provide a promising solution to indoor positioning, orientating and navigation particularly when the global positioning system is unaccessible [5], [6].

A multitude of VLC-based localization methods were proposed, e.g., inertial measurement unite (IMU) [7], time-of-arrival [8], angle-of-arrival [2], and received signal strength (RSS)-related ones [9], in various environments. Among these methods, the RSS-based method is simple and widely accessible, which can be used to enhance VLC localization. However, there are still several technical challenges that need to be addressed, as elaborated in the following.

1) Orientation: In VLCs, RSS depends on the transmission distance, the incidence direction and the transceiver's orientation states [9], [10]. Thus, in addition to the user equipment (UE) position, the unknown orientation of UE also needs to be estimated. This makes VLC-based positioning very difficult, due to the increased uncertainty in parameters. In [2], [11] and [12], the UE orientation[1] is assumed known to simplify the positioning problem. In [12], a narrow field-of-view (FoV) of transmitters was assumed to exploit angular knowledge for positioning. In [14], both transmitters and receiver (i.e., UE) are assumed with perpendicular orientations to room ceiling. Also, the knowledge of UE height is required to derive UE position. Similarly, an upward orientation of UE is required in [15]. In [16], an IMU sensor is required to measure the UE tilt angle. In these works, some priori knowledge or special requirements are needed.

2) Positioning: Since RSS model is nonlinear with respect to (w.r.t.) UE position [16], [17], the VLC-based positioning is a non-convex problem with lots of local optima. Thus, the VLC-based positioning is very challenging, despite several approaches were proposed previously. For instance, a data-driven Bayesian positioning approach was proposed in [18]. This approach is based on an assumption that measurement samples are correlated in spatial-domain, and a Gaussian kernel is employed to acquire such correlation. Thus, prior to UE localization, a labor-intensive site survey is required to train the Gaussian kernel model. A least square-based Newton-Raphson method was proposed in [9] to estimate UE location. This method converges to a locally optimal solution. For the non-convex problem with lots of local optima, there would be a large estimation error when the obtained local optimum solution is far away from the global optimum.

The particle swarm optimization (PSO) provides an effective solution to non-convex optimization [19]–[22]. It uses random particles to explore the update knowledge at each iteration.

This work was supported by Science and Technology Plan of Shenzhen (JCYJ20170818114014753). Qingchun Chen's work was supported by NSFC under grant No.61771406.

[1]For brevity, we use "UE orientation" to denote the orientation of the VLC receiver axis, which will be explicitly explained in Section II.

However, there still remains the potential to further improve the convergence rate by exploring potential update knowledge. In addition, a sophisticated update-decision mechanism is desired to ensure the convergence. Simulated annealing (SA) provides an alternative approach for non-convex optimization. It employs a stochastic update scheme to ensure a weak global convergence [23]–[25]. However, the candidate update of SA particles is randomly generated without any guidance, which leads to a low convergence rate.

3) Performance Limits: The performance of RSS-based positioning was studied previously. In [26] the Cramer-Rao lower bound (CRLB) on distance estimation error was studied, and the impact of multipath reflection was considered. Similarly, in [27], the CRLB for angular diversity-enhanced positioning was derived. Besides RSS, the performance of time-of-arrival-based VLC positioning was studied in [8] and [28]. However, all these analyses focused on positioning error performance only, and extension of the analysis to SPAO is not trivial.

In this paper, we shall focus on the three-dimensional SPAO of VLC based on RSS measurements. The contributions of this paper are four-fold, as summarized below.

- [**An Efficient SPAO Scheme**] Firstly, an efficient SPAO scheme to achieve both location and orientation estimate for the VLC-based localization is proposed, which does not require any priori knowledge of UE height, transceiver orientation alignment or inertial measurement units. Thus, it is very applicable to practical VLC localization. This is a significant technical improvement over the existing VLC localization solutions in [11]–[16].
- [**A Novel PASS Algorithm**] Secondly, a novel algorithm named particle-assisted stochastic search (PASS) is proposed to address the non-convex SPAO problem (with lots of local optima). Unlike the traditional PSO algorithm and its variations [19], the proposed PASS algorithm exploits the multi-scale search mechanism (i.e., global search, local detection and historical information) and the stochastic update scheme with problem-specific update rule design to find the globally optimal solution. It is shown that the proposed PASS algorithm can achieve a high-accuracy solution for VLC-based SPAO.
- [**Convergence Analysis of PASS**] Thirdly, we establish the convergence of the proposed PASS algorithm, which justifies the PASS-based SPAO scheme. It will be shown that the PASS algorithm will converge in probability to the globally optimal solution to the SPAO problem, which is superior to conventional gradient-based methods that only ensures convergence to a local optimal solution.
- [**Closed-Form Performance Analysis**] Fourthly, we derive a closed-from CRLB on position and orientation errors of the RSS-based SPAO for VLCs. We show that both position and orientation accuracies scale linearly with signal-to-noise-ratio (SNR). In addition, position and orientation accuracies decay with transmission distance in the sixth and fourth powers, respectively.

The remainder of this paper is organized as follows. Section II presents system model. The PASS algorithm is proposed in Section III. In Section IV, algorithmic convergence is analyzed. CRLB analysis is conducted in Section V. Simulations results are presented in Section VI. Section VII concludes the paper.

II. System Model

In this section, we elaborate the physical setup and measurement model of SPAO for VLC systems.

A. Physical Setup

We consider a VLC-based localization system with M light-emitting diode (LED) transmitters and a static VLC receiver equipped with photodiodes (i.e., UE), as illustrated in Fig. 1. We use $\mathbf{p}_m \in \mathbb{R}^3$ and $\mathbf{v}_m \in \mathbb{R}^3$ to denote the location and orientation[2] of the mth LED transmitter, respectively, for $m = 1, \cdots, M$. These LEDs will act as anchors for UE localization, and their locations and orientations are known. In addition, let $\mathbf{x}_R \in \mathbb{R}^3$ and $\mathbf{u}_R \in \mathbb{R}^3$ denote the UE position and orientation, respectively, which are unknown.

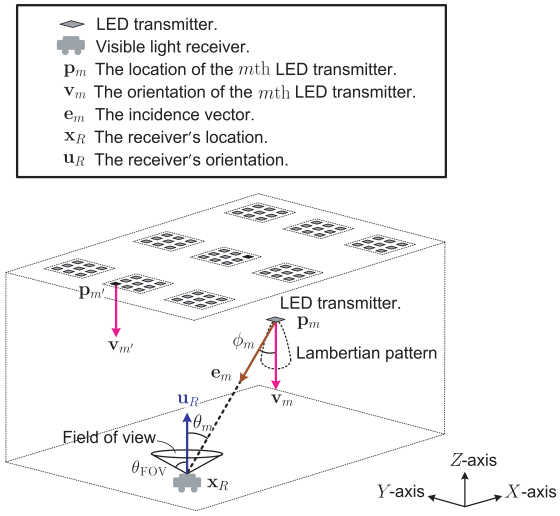

Fig. 1. Illustration of the VLC-based SPAO system.

When LED emitters turn on for illumination, they periodically communicate with UE for data transmission. During this period, if UE attempts to determine its own location $\mathbf{x}_R$ and orientation $\mathbf{u}_R$, it will first acquire the identifications (IDs) of observed LED transmitters and the strength of received VLC signals. Then, based on the LED IDs, the LED locations and orientations, the RSS measurements and the RSS model knowledge (elaborated later), the UE location and orientation will be simultaneously determined.

To ensure the effectiveness of the above VLC-based localization procedure, we assume the VLC protocol [29] (*e.g.*, IEEE 802.15.7) and the multiple access method [30] (e.g., time-division one) have been well defined by the VLC system.

B. Measurement Model

The RSS of VLC is dependent on radiation, incidence angle gain, transmission distance, emitting power and characteristic constants. We assume all LEDs have the same emitting power,

[2]LED orientation means its main emitting direction, as shown in Fig. 1.

denoted by W_T. The radiation of LEDs is usually described by a Lambertian pattern [5] characterized by a Lambertian order $r = -\dfrac{\ln 2}{\ln\cos(A_{\frac{1}{2}})}$, where $A_{\frac{1}{2}}$ is the semi-angle at half power of LEDs [31]. For a typical LED with an illumination range within $[-\pi/3, \pi/3]$ (i.e., $A_{\frac{1}{2}} = \pi/3$), usually $r = 1$ [32]. For the photodiode of UE, we assume its aperture, optical filter gain and optical concentrator gain are Ψ_R, G_R and Γ_R, respectively, where $\Gamma_R = \dfrac{\zeta_R^2}{(\sin(\theta_{\rm FOV}))^2}$ if UE's incidence angle $\theta_m \in [0, \theta_{\rm FOV}]$, and zero otherwise, in which ζ_R denotes the refractive index of UE optical concentrator and $\theta_{\rm FOV}$ denotes the UE's FoV [16], as shown in Fig. 1.[3]

Then, for an UE at $\mathbf{x}_R$ with $\mathbf{u}_R$, its RSS ($i.e.$, direct current gain) is given by the following general form,

$$\mathrm{z}_m = h_m\big(\mathbf{x}_R, \mathbf{u}_R\big) + \varsigma_{\mathsf{nlos},m} + \epsilon_m,\ \forall m \in \Omega_R, \tag{1}$$

where $\epsilon_m \sim \mathcal{N}\big(\epsilon_m|0, \omega_m\big)$ is the measurement noise, which is generally assumed to be an i.i.d. zero-mean Gaussian variable [33], [34], [35] with precision ω_m (i.e., the inverse of variance that quantifies the accuracy), $h_m\big(\mathbf{x}_R, \mathbf{u}_R\big)$ is the measurement function associated with line-of-sight (LOS) signal (elaborated later), $\varsigma_{\mathsf{nlos},m}$ denotes the strength of non-line-of-sight (NLOS) signals, and Ω_R is the set of LEDs whose light can reach UE, given by $\Omega_R = \big\{m\big|\big|\frac{\theta_m}{\theta_{\rm FOV}}\big| \le 1, \big|\frac{\phi_m}{\pi/2}\big| \le 1, \forall m = 1:M\big\}$, where $\phi_{\rm FOV}$ is LED's FoV, θ_m is the incidence angle between $\mathbf{u}_R$ and incidence vector $\mathbf{e}_m$, and ϕ_m is the irradiance angle between $\mathbf{v}_m$ and $\mathbf{e}_m$ that is given by

$$\mathbf{e}_m = \frac{\mathbf{x}_R - \mathbf{p}_m}{\|\mathbf{x}_R - \mathbf{p}_m\|_2}. \tag{2}$$

For the LOS channel, the associated measurement function $h_m\big(\mathbf{x}_R, \mathbf{u}_R\big)$ is usually given by [9]

$$h_m\big(\mathbf{x}_R, \mathbf{u}_R\big) = \frac{\Gamma_R G_R W_T \Psi_R}{2\pi} \frac{(r+1)\big(\cos\big(\phi_m\big)\big)^r \cos\big(\theta_m\big)}{\|\mathbf{x}_R - \mathbf{p}_m\|_2^2}, \tag{3}$$

where W_T, G_R, Γ_R and Ψ_R are model constants independent of the UE location and orientation. For brevity, let $\Psi'_R = \dfrac{\Gamma_R W_T G_R \Psi_R}{2\pi}$. For the NLOS component $\varsigma_{\mathsf{nlos},m}$, there are a number of works on its modeling, e.g., [36]–[40]. However, these NLOS models are still complicated and depend on some ideal assumptions (e.g., empty cuboid room) or perfect knowledge of some physical parameters (e.g., reflectance of walls) that are hard to be fulfilled in practice. Hence, to achieve a good balance between model complexity and localization accuracy, we adopt the LOS component to localize UE since it has simple model and it is dominant in most cases. This model has been widely adopted in literature, for instance, [6], [16], [41]. In addition, we assume there is no knowledge of the relationship between $\varsigma_{\mathsf{nlos},m}$ and UE location parameter $\{\mathbf{x}_R, \mathbf{u}_R\}$ due to their complex dependency, and thus we consider $\varsigma_{\mathsf{nlos},m}$ as a disturbance source (without any informative contribution to UE location estimate).

In addition, given LED location $\mathbf{p}_m$ and orientation $\mathbf{v}_m$, the incidence angle θ_m and irradiance angle ϕ_m are related to UE position $\mathbf{x}_R$ and orientation $\mathbf{u}_R$ as follows,

$$\phi_m = \arccos\left(\frac{(\mathbf{x}_R - \mathbf{p}_m)^\top \mathbf{v}_m}{\|\mathbf{x}_R - \mathbf{p}_m\|_2 \|\mathbf{v}_m\|_2}\right), \tag{4}$$

$$\theta_m = \arccos\left(\frac{(\mathbf{p}_m - \mathbf{x}_R)^\top \mathbf{u}_R}{\|\mathbf{x}_R - \mathbf{p}_m\|_2 \|\mathbf{u}_R\|_2}\right), \tag{5}$$

where $\bullet^\top$ is the transpose. Thus, the measurement function $h_m\big(\mathbf{x}_R, \mathbf{u}_R\big)$ in (3) can be rewritten as an explicit function of $\mathbf{x}_R$ and $\mathbf{u}_R$ as shown in (6) (on the top of next page).

C. Problem Formulation of SPAO

The goal of VLC-based SPAO is to simultaneously estimate UE position $\mathbf{x}_R$ and orientation $\mathbf{u}_R$ from $\big\{\mathrm{z}_m|\forall m \in \Omega_R\big\}$.

Based on the maximum likelihood criterion, the receiver location and orientation are estimated as follows,

$$\big(\hat{\mathbf{x}}_R, \hat{\mathbf{u}}_R\big) = \underset{\mathbf{x}_R, \mathbf{u}_R}{\arg\max}\ p(\mathbf{z}|\mathbf{x}_R, \mathbf{u}_R), \tag{7}$$

where $\mathbf{z} = \mathrm{vec}[\mathrm{z}_m|\forall m \in \Omega_R]$ is the measurement vector with $\mathrm{vec}[\bullet]$ yielding a column vector, and the likelihood function $p(\mathbf{z}|\mathbf{x}_R, \mathbf{u}_R)$ is given by

$$p(\mathbf{z}|\mathbf{x}_R, \mathbf{u}_R) = \prod_{m \in \Omega_R} \mathcal{N}\big(\mathrm{z}_m|h_m(\mathbf{x}_R, \mathbf{u}_R), \omega_m\big). \tag{8}$$

Remark 1. SPAO is challenging since $p(\mathbf{z}|\mathbf{x}_R, \mathbf{u}_R)$ is a non-convex function with respect to (w.r.t.) $\mathbf{x}_R$ and $\mathbf{u}_R$. □

Therefore, a novel particle-assisted stochastic search (PASS) algorithm is proposed to provide an efficient solution.

III. THE PASS-BASED SPAO SCHEME

Let $\boldsymbol{\alpha}_R = \begin{bmatrix} \mathbf{x}_R \\ \mathbf{u}_R \end{bmatrix}$ be the collection of unknown UE location and orientation. To handle the non-convex SPAO problem, a set of random samples (named search particle set) $\big\{\boldsymbol{\alpha}_k(n), \varphi_k(n)|\forall n = 1:N_S\big\}$ are used to iteratively find the globally optimal solution $\hat{\boldsymbol{\alpha}}_R$, where $\boldsymbol{\alpha}_k(n)$ denotes the nth search particle, $\varphi_k(n)$ stands for its belief, n is the search particle index, N_S denotes the total number of search particles, and k stands for the iteration index.

The initial search particles (when $k = 1$) are uniformly generated within the feasible area, since there is no priori information of UE location and orientation.

At the kth iteration, each search particle $\boldsymbol{\alpha}_k(n)$ will generate a candidate update $\boldsymbol{\alpha}_k^\flat(n)$ based on a multi-scale search mechanism. Then, the candidate update $\boldsymbol{\alpha}_k^\flat(n)$ will be approved or rejected, according to a stochastic update-decision scheme. An illustration of the PASS algorithm is given in Fig. 2. Unlike traditional PSO algorithms, the PASS algorithm uses a multi-scale search mechanism (mainly including global search and local detection) to explore diverse update knowledge to improve the evolution efficiency, and a stochastic update decision mechanism is used to ensure the convergence.

In the following, we shall elaborate the multi-scale search-based candidate update generation and the stochastic update.

[3] Typically, $G_R = 1$, $\zeta_R = 1.5$, $\Psi_R = 1\,[\mathrm{cm}^2]$ and $\theta_{\rm FOV} = \pi/2$ [16], and the other parameter settings will be specified in simulations.

$$h_m\big(\mathbf{x}_R, \mathbf{u}_R\big) = -\Psi'_R \frac{(r+1)\left((\mathbf{x}_R - \mathbf{p}_m)^\top \mathbf{v}_m\right)^r (\mathbf{x}_R - \mathbf{p}_m)^\top \mathbf{u}_R}{\|\mathbf{x}_R - \mathbf{p}_m\|_2^{r+3} \|\mathbf{v}_m\|_2^r \|\mathbf{u}_R\|_2}. \tag{6}$$

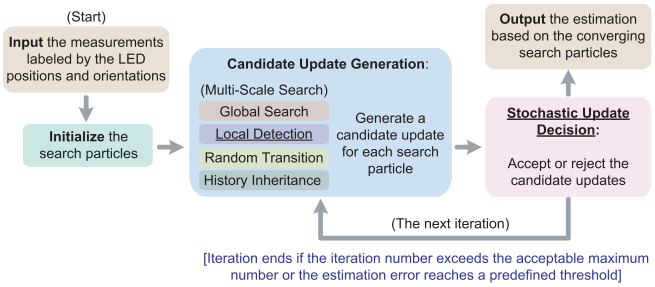

Fig. 2. The mechanism of the proposed PASS algorithm, where the principal novel components compared with PSO are highlighted by using underlines.

A. Candidate Update Generation

Given a search particle $\boldsymbol{\alpha}_k(n)$, $\forall n = 1 : N_S$, at the kth iteration, its candidate update $\boldsymbol{\alpha}_k^\flat(n)$ is determined by

$$\boldsymbol{\alpha}_k^\flat(n) = \boldsymbol{\alpha}_k(n) + L_0 \boldsymbol{\upsilon}_k(n) + \boldsymbol{\mu}_k(n), \tag{9}$$

and its candidate update belief $\varphi_k^\flat(n)$ is given by

$$\varphi_k^\flat(n) = p\big(\mathbf{z}|\boldsymbol{\alpha}_k^\flat(n)\big), \tag{10}$$

where $L_0 \in (0,1)$ denotes the search step length, and $\boldsymbol{\mu}_k(n)$ is the random transition vector that will be explicated in Eq. (24). In addition, $\boldsymbol{\upsilon}_k(n)$ denotes the evolution vector of the search particle $\boldsymbol{\alpha}_k(n)$, which is given by

$$\boldsymbol{\upsilon}_k(n) = \lambda_0 \boldsymbol{\upsilon}_{k-1}(n) + \widetilde{\boldsymbol{\upsilon}}_k(n), \tag{11}$$

$$\widetilde{\boldsymbol{\upsilon}}_k(n) = \lambda_1\big(\boldsymbol{\alpha}_k^{\mathrm{GB}} - \boldsymbol{\alpha}_k(n)\big) + \lambda_2\big(\boldsymbol{\alpha}_k^{\mathrm{LB}}(n) - \boldsymbol{\alpha}_k(n)\big), \tag{12}$$

where $\boldsymbol{\alpha}_k^{\mathrm{GB}}$ is the globally best particle, $\lambda_0 \in [0,1)$ is an inheritance factor, $\boldsymbol{\alpha}_k^{\mathrm{LB}}(n)$ is the locally best particle of search particle $\boldsymbol{\alpha}_k(n)$ (i.e., the maximum-belief point in a small area around the current search particle), and λ_1, λ_2 are two positive weighting factors satisfying $0 < \lambda_1 + \lambda_2 \leq 1$. Then, $\lambda_0 \boldsymbol{\upsilon}_{k-1}(n)$ stands for the "historical update knowledge".

In the following, we shall elaborate the multi-scale search scheme in the proposed PASS algorithm, including "global search", "local detection" and "random transition".

1) Global Search: The globally best particle $\boldsymbol{\alpha}_k^{\mathrm{GB}}$ in (12) is defined as the search particle with the highest belief,

$$\boldsymbol{\alpha}_k^{\mathrm{GB}} = \underset{\boldsymbol{\alpha}_k(n)|\forall n=1:N_S}{\arg\max} \big\{\varphi_k(n)|\forall n = 1 : N_S\big\}, \tag{13}$$

where each search particle belief $\varphi_k(n)$ is calculated as

$$\varphi_k(n) = p\big(\mathbf{z}|\boldsymbol{\alpha}_k(n)\big). \tag{14}$$

This global search is to exploit the globally best update knowledge within the coverage area of the search particles.

2) Local Detection: The locally best particle $\boldsymbol{\alpha}_k^{\mathrm{LB}}(n)$ in (12) means the maximum-belief detection particle,

$$\boldsymbol{\alpha}_k^{\mathrm{LB}}(n) = \underset{\boldsymbol{\alpha}_k^{(\tau)}(n)|\tau=1:N_D}{\arg\max} \big\{\wp_k^{(\tau)}(n)|\forall \tau = 1 : N_D\big\}, \tag{15}$$

where $\wp_k^{(\tau)}(n)$ is the belief of detection particle $\boldsymbol{\alpha}_k^{(\tau)}(n)$, and N_D is the number of detection particles of each search particle. In addition, the detection belief $\wp_k^{(\tau)}(n)$ is calculated as

$$\wp_k^{(\tau)}(n) = p\big(\mathbf{z}|\boldsymbol{\alpha}_k^{(\tau)}(n)\big). \tag{16}$$

In order to find the locally best particle $\boldsymbol{\alpha}_k^{\mathrm{LB}}(n)$, a set of random samples $\{\boldsymbol{\alpha}_k^{(\tau)}(n), \wp_k^{(\tau)}(n)|\forall \tau = 1 : N_D\}$, named the detection particle set, is used for each search particle $\boldsymbol{\alpha}_k(n)$.

In the following, we shall address the generation of detection particles. For convenience, we need to partition the detection particle $\boldsymbol{\alpha}_k^{(\tau)}(n)$ as $\boldsymbol{\alpha}_k^{(\tau)}(n) = \begin{bmatrix} \mathbf{x}_k^{(\tau)}(n) \\ \mathbf{u}_k^{(\tau)}(n) \end{bmatrix}$, where $\mathbf{x}_k^{(\tau)}(n)$ and $\mathbf{u}_k^{(\tau)}(n)$ denote the τth detection particle associated with $\mathbf{x}_R$ and $\mathbf{u}_R$, respectively. Similarly, each search particle $\boldsymbol{\alpha}_k(n)$ is partitioned as $\boldsymbol{\alpha}_k(n) = \begin{bmatrix} \mathbf{x}_k(n) \\ \mathbf{u}_k(n) \end{bmatrix}$, where $\mathbf{x}_k(n)$ and $\mathbf{u}_k(n)$ stand for the position search particle and orientation search particle, respectively.

• **Local Detection of Position**. Firstly, the position detection particles are random samples on a spherical surface centered at the location search particle $\mathbf{x}_k(n)$, with a radius $L_1(n)$,

$$\mathbf{x}_k^{(\tau)}(n) = \mathbf{x}_k(n) + L_1(n) \frac{\boldsymbol{x}_k^{(\tau)}(n)}{\|\boldsymbol{x}_k^{(\tau)}(n)\|_2}, \tag{17}$$

$$\boldsymbol{x}_k^{(\tau)}(n) \sim \mathcal{N}\big(\boldsymbol{x}_k^{(\tau)}(n)|\mathbf{0}, \mathbf{I}_3\big),\ \forall \tau = 1 : N_D, \tag{18}$$

where $\mathbf{I}_3$ denotes the 3×3 identity matrix, $\boldsymbol{x}_k^{(\tau)}(n)$ is a basic sample, and $L_1(n) \in (0,1)$ satisfies $\lim\limits_{N\to\infty} L_1(n) = 0$ and $\lim\limits_{N\to\infty} \sum\limits_{n=1:N} L_1(n) = \infty$ (infinite travel). Namely, we use a set of random vectors with a unit length to generate the detection particles around the corresponding search particles.

• **Local Detection of Orientation**. Secondly, the orientation detection particles are random samples (which will be illustrated in Fig. 3) on a circle centered at the corresponding orientation search particle, *i.e.*,

$$\mathbf{u}_k^{(\tau)}(n) = \mathbf{u}_k(n) + L_2(n) \boldsymbol{\Lambda}_k(n) \mathbf{g}_k^{(\tau)}(n), \tag{19}$$

where $L_2(n) \in (0,1)$ is the orientation detection step length satisfying $\lim\limits_{N\to\infty} L_2(n) = 0$ and $\lim\limits_{N\to\infty} \sum\limits_{n=1:N} (L_2(n)) = \infty$, and $\mathbf{g}_k^{(\tau)}(n)$ denotes the orientation's basic random sample uniformly distributed on a unit-radius circle,

$$\mathbf{g}_k^{(\tau)}(n) = \begin{bmatrix} \cos\left(\vartheta_k^{(\tau)}(n)\right) \\ \sin\left(\vartheta_k^{(\tau)}(n)\right) \\ 0 \end{bmatrix}, \tag{20}$$

where $\vartheta_k^{(\tau)}(n)$ is a random angle sample, and

$$\vartheta_k^{(\tau)}(n) \sim \mathrm{rand}(0, 2\pi),\ \forall \tau = 1 : N_D, \tag{21}$$

In addition, $\mathbf{\Lambda}_k(n)$ denotes the rotation matrix dependent on the orientation search particle $\mathbf{u}_k(n)$, which is given by

$$\mathbf{\Lambda}_k(n) = \mathbf{\Phi}_k^{\star}(n)\Big(\mathbf{\Phi}_k'(n)\big(\mathbf{\Phi}_k'(n)\big)^{\top}\Big)^{\dagger}\mathbf{\Phi}_k'(n)\big(\mathbf{\Phi}_k''(n)\big)^{\top},$$

where $\bullet^{\dagger}$ is the pseudo-inverse, and $\mathbf{\Phi}_k^{\star}(n)$, $\mathbf{\Phi}_k'(n)$ and $\mathbf{\Phi}_k''(n)$ are given by $\mathbf{\Phi}_k^{\star}(n) = \begin{bmatrix} \cos\big(\varrho_k(n)\big) & -\sin\big(\varrho_k(n)\big) & 0 \\ \sin\big(\varrho_k(n)\big) & \cos\big(\varrho_k(n)\big) & 0 \\ 0 & 0 & 1 \end{bmatrix}$, $\mathbf{\Phi}_k'(n) = \begin{bmatrix} \cos\big(\psi_k(n)\big) & 0 \\ 0 & 1 \\ -\sin\big(\psi_k(n)\big) & 0 \end{bmatrix}$ and $\mathbf{\Phi}_k''(n) = \begin{bmatrix} 1 & 0 \\ 0 & 1 \\ 0 & 0 \end{bmatrix}$, respectively, where $\psi_k(n)$ and $\varrho_k(n)$ denote the rotation angles around the Y- and Z-axis, respectively, which are given by

$$\varrho_k(n) = \mathrm{sign}\Big(\big(\mathbf{u}_k^X(n)\big)^{\top}\mathbf{e}_Y\Big)\arccos\Big(\big(\mathbf{u}_k^X(n)\big)^{\top}\mathbf{e}_X\Big), \quad (22)$$

$$\psi_k(n) = \arccos\big((\mathbf{u}_k(n))^{\top}\mathbf{e}_Z\big), \quad (23)$$

where $\mathbf{e}_X = [1,0,0]^{\top}$, $\mathbf{e}_Y = [0,1,0]^{\top}$ and $\mathbf{e}_Z = [0,0,1]^{\top}$ are the basis vectors on the X-, Y- and Z-axis, respectively, and $\mathrm{sign(x)}$ is the sign function. In addition, $\mathbf{u}_k^X(n)$ is the projection of $\mathbf{u}_k(n)$ on the XY-plane, $\mathbf{u}_k^X(n) = \begin{bmatrix} [\mathbf{u}_k(n)]_1 \\ [\mathbf{u}_k(n)]_2 \\ 0 \end{bmatrix}$, where $[\mathbf{u}_k(n)]_i$ is the ith element of $\mathbf{u}_k(n)$, and $i = 1, 2$.

Remark 2. The rotation matrix $\mathbf{\Lambda}_k(n)$ is used to rotate basic random samples $\big\{\mathbf{g}_k^{(\tau)}(n)|\forall\tau = 1 : N_D\big\}$ by angle $\psi_k(n)$ around the Y-axis first, and then rotate them by angle $\varrho_k(n)$ around the Z-axis, eventually forming the random samples $\big\{\mathbf{\Lambda}_k(n)\mathbf{g}_k^{(\tau)}(n)|\forall\tau = 1 : N_D\big\}$. The rotation matrix $\mathbf{\Lambda}_k(n)$ is used to guarantee the orientation detection particles in a plane orthogonal to the orientation search particle $\mathbf{u}_k(n)$. The basic random samples $\big\{\mathbf{g}_k^{(\tau)}(n)|\forall\tau = 1 : N_D\big\}$ with a uniform distribution preserve the diversity of detection direction. □

The orientation detection particle is illustrated in Fig. 3, where $\varrho_k(n)$ denotes the azimuth angle of orientation search particle $\mathbf{u}_k(n)$, and $\psi_k(n)$ is its polar angle.

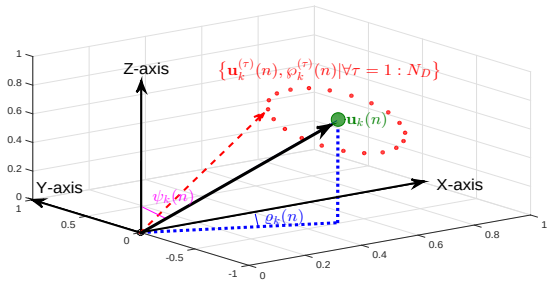

Fig. 3. The orientation detection particles $\big\{\mathbf{u}_k^{(\tau)}(n)|\forall\tau = 1 : N_D\big\}$.

Once obtaining $\{\mathbf{x}_k^{(\tau)}(n), \mathbf{u}_k^{(\tau)}(n)|\forall\tau = 1 : N_D\}$ as above, $\{\boldsymbol{\alpha}_k^{(\tau)}(n)|\forall\tau = 1 : N_D\}$ is determined. Then, the locally best particle $\boldsymbol{\alpha}_k^{\mathrm{LB}}(n)$ of $\boldsymbol{\alpha}_k(n)$ can be determined as per (15).

3) Random Transition: In Eq. (9), the random transition vector $\boldsymbol{\mu}_k(n)$ w.r.t. the search particle $\boldsymbol{\alpha}_k(n)$ is given by

$$\boldsymbol{\mu}_k(n) \sim \mathcal{N}\big(\boldsymbol{\mu}_k(n)|\mathbf{0}, \mathbf{H}_k(n)\big), \quad (24)$$

where $\mathbf{H}_k(n)$ is the transition precision matrix. A high randomness can be imposed on the transition of poor search particles, *i.e.*, $\mathbf{H}_k(n) \preceq \mathbf{H}_k(n')$ if $\varphi_k(n) \leq \varphi_k(n')$, which can be achieved through assigning a precision matrix to search particles as per their searching beliefs' partial order at each iteration. This random factor allows PASS to be able to escape from the local optimum with some probability.

After determining the globally best particle $\boldsymbol{\alpha}_k^{\mathrm{GB}}$, the locally best particle $\boldsymbol{\alpha}_k^{\mathrm{LB}}(n)$ and the random transition $\boldsymbol{\mu}_k(n)$ based on Eqs. (13), (15) and (24), respectively, each search particle $\boldsymbol{\alpha}_k(t)$ can generate a candidate update $\boldsymbol{\alpha}_k^{\flat}(n)$, $\forall n = 1 : N_S$, based on Eqs. (9)–(12). In the following we aim to explicate the mechanism on how to determine the eventual update of each search particle, given the associated candidate update.

B. Stochastic Update Decision

Consider a candidate update $\boldsymbol{\alpha}_k^{\flat}(n)$ of the search particle $\boldsymbol{\alpha}_k(n)$ at the kth iteration. If $\boldsymbol{\alpha}_k^{\flat}(n)$ is a good candidate update with a non-decreased belief, it will be approved directly, *i.e.*,

$$\boldsymbol{\alpha}_{k+1}(n) = \boldsymbol{\alpha}_k^{\flat}(n), \text{ if } \varphi_k^{\flat}(n) \geq \varphi_k(n), \quad (25)$$

where $\varphi_k^{\flat}(n)$ and $\varphi_k(n)$ are the beliefs associated with $\boldsymbol{\alpha}_k^{\flat}(n)$ and $\boldsymbol{\alpha}_k(n)$, respectively, which are given by Eqs. (10) and (14). Otherwise, $\boldsymbol{\alpha}_k^{\flat}(n)$ is a bad candidate update and will be accepted according to the following probability p_{a}

$$p_{\mathrm{a}} = \exp\left(-\frac{\varphi_k(n) - \varphi_k^{\flat}(n)}{\mathcal{T}\left(\varphi_k(n)\right)}k\right), \quad (26)$$

where $\mathcal{T}(\varphi_k(n))$ stands for a decreasing "temperature" function with respect to $\varphi_k(n)$, which is defined as

$$\mathcal{T}\left(\varphi_k(n)\right) = c_1 \exp\left(-c_2\frac{\varphi_k(n)}{\varphi_k^{\star}}\right)\varphi_k(n), \quad (27)$$

where c_1 and c_2 denote two positive constants, and $\varphi_k^{\star}$ denotes the belief of the globally best particle $\boldsymbol{\alpha}_k^{\mathrm{GB}}$ (given by Eq. (13)) at the kth iteration. We can observe that a worse candidate update will correspond to a lower acceptance probability.

Specifically, for a bad candidate update, a uniform random number $a \sim \mathrm{rand}(0,1)$ is generated first. If $a \leq p_{\mathrm{a}}$, the bad candidate update $\mathbf{x}_k^{\flat}(n)$ is accepted, *i.e.*,

$$\boldsymbol{\alpha}_{k+1}(n) = \boldsymbol{\alpha}_k^{\flat}(n), \text{ if } \varphi_k^{\flat}(n) < \varphi_k(n) \text{ and } a \leq p_{\mathrm{a}}. \quad (28)$$

Otherwise, $\boldsymbol{\alpha}_k^{\flat}(n)$ is dropped, and the search particle keeps its original state $\boldsymbol{\alpha}_k(n)$ in the next iteration, *i.e.*,

$$\boldsymbol{\alpha}_{k+1}(n) = \boldsymbol{\alpha}_k(n), \text{ if } \varphi_k^{\flat}(n) < \varphi_k(n) \text{ and } a > p_{\mathrm{a}}. \quad (29)$$

The idea of the stochastic update decision is to approve a good candidate update directly, and to accept a bad candidate update with a probability that is cooling down over iterations.

Remark 3. The candidate update benefits from global search, local detection and historical inheritance, which form a multi-scale probe to explore diverse update knowledge. In addition, a random transition is imposed on the candidate update. The poorer the particles, the larger the random factors. Moreover, a probability-cooling stochastic update scheme is used to determine the search particle evolution, where poorer particles

are endowed with a larger chance of accepting a worse update, which provides an opportunity to jump from a local optimum point. Thanks to the multi-scale search, random transition and stochastic update, the PASS algorithm can achieve a balance between exploration and exploitation to capture the global optimum solution. The key points are summarized as follows.

- The lower the search belief is, the larger the associated random factor becomes.
- The worse the candidate update is, the lower the associated acceptance probability becomes.
- The earlier the iteration is, the greater the acceptance probability of bad candidate updates becomes.
- The lower the search belief is, the greater the acceptance probability of bad candidate updates is. □

C. The PASS-based SPAO Estimator

Given the search particle set $\{\boldsymbol{\alpha}_k(n), \varphi_k(n)|\forall n = 1 : N_S\}$, an approximate minimum mean square error estimation is obtained at each iteration,

$$\hat{\boldsymbol{\alpha}}_k = \sum_{n=1:N_S} \varphi_k(n)\boldsymbol{\alpha}_k(n), \tag{30}$$

where we assume the searching beliefs are normalized at the estimation step, *i.e.*, $\varphi_k(n) = \dfrac{\varphi_k(n)}{\sum\limits_{n'=1:N_S} \varphi_k(n')}$, $\forall n = 1 : N_S$.

At the kth iteration, the receiver location and orientation are estimated as $\hat{\mathbf{x}}_k = [\hat{\boldsymbol{\alpha}}_k]_{1:3}$ and $\hat{\mathbf{u}}_k = [\hat{\boldsymbol{\alpha}}_k]_{4:6}$, respectively.

Given signal propagation parameters (*e.g.*, $\theta_{\rm FOV}$, r, Ψ_R, N_S and N_D), the receiver location $\mathbf{x}_R$ and orientation $\mathbf{u}_R$ can be iteratively identified, based on the proposed PASS algorithm. The associated pseudo-codes are presented in **Algorithm 1**.

Computational Complexity. The complexity of the proposed PASS algorithm is $\mathcal{O}\big(N_S N_D|\Omega_R|K\big)$, where $|\Omega_R|$ is the size of Ω_R, and K is the number of iterations. Usually, N_S and N_D lower than 50 are enough for a robust SPAO performance in the three-dimensional case. The complexities of the PSO [22] and SA algorithms [25] scale as $\mathcal{O}(N_S|\Omega_R|K)$. The practically consumed CPU time of various algorithms will be elaborated and compared in simulation section.

Algorithm 1: The proposed PASS-based SPAO scheme

Input : $\mathbf{p}_m, \mathbf{v}_m, \mathrm{z}_m, \forall m = 1 : M$.
Determine algorithm parameters, e.g., $N_S, N_D, \lambda_0 \cdots \lambda_2$.
Collect all measurement signals $\big\{\mathrm{z}_m|\forall m \in \Omega_R\big\}$.
Generate initial search particles $\big\{\boldsymbol{\alpha}_1(n)|\forall n = 1 : N_S\big\}$.
While not converge **do** (*i.e.*, $k = 1, 2, \cdots$)
  For $n = 1 : N_S$ **do**
    Calculate the searching belief $\varphi_k(n)$ of each search particle $\boldsymbol{\alpha}_k(n)$, based on Eq. (14).
  End
  Return the estimate $\hat{\boldsymbol{\alpha}}_k$, $\hat{\mathbf{x}}_k$ and $\hat{\mathbf{u}}_k$.
  Find the globally best particle $\boldsymbol{\alpha}_k^{\rm GB}$, based on (13).
  For $n = 1 : N_S$ **do**
    Generate detection particle $\boldsymbol{\alpha}_k^{(\tau)}(n), \tau = 1 : N_D$.
    Calculate detection belief $\wp_k^{(\tau)}(n), \tau = 1 : N_D$.
    Find the locally best particle $\boldsymbol{\alpha}_k^{\rm LB}(n)$.
    Generate candidate update $\boldsymbol{\alpha}_k^\flat(n)$ based on (9).
    Calculate the associated update belief $\varphi_k^\flat(n)$.
    If the update is better, *i.e.*, $\varphi_k^\flat(n) \geq \varphi_k(n)$,
      Approve the update $\boldsymbol{\alpha}_{k+1}(n) = \boldsymbol{\alpha}_k^\flat(n)$.
    Else Generate $a \sim \mathrm{rand}(0, 1)$.
      If $a \leq \exp\left(-\dfrac{\varphi_k(n) - \varphi_k^\flat(n)}{\mathcal{T}\left(\varphi_k(n)\right)}k\right)$, then
        Approve the update $\boldsymbol{\alpha}_{k+1}(n) = \boldsymbol{\alpha}_k^\flat(n)$.
      Else
        Keep it fixed $\boldsymbol{\alpha}_{k+1}(n) = \boldsymbol{\alpha}_k(n)$.
      End
    End
  End
End
Return the final estimate $\hat{\mathbf{x}}_R = \hat{\mathbf{x}}_k$ and $\hat{\mathbf{u}}_R = \hat{\mathbf{u}}_k$.
Output: $\hat{\mathbf{x}}_R$ and $\hat{\mathbf{u}}_R$.

IV. Convergence Analysis

The convergence of the proposed PASS algorithm associated with N_S and iteration number k is established in this section.

A. Previous Work

In [42], the convergence of SA over a discrete state space was demonstrated for a deterministic temperature cooling schedule, where the acceptance probability of a bad update is given by $p_{\rm a} = \exp\left(-\dfrac{\varphi_k(n) - \varphi_k^\flat(n)}{\mathrm{Tem}\,(k)}\right)$ and the cooling schedule is $\mathrm{Tem}\,(k) = \dfrac{c}{\log(1+k)}$ with c being a dependent parameter. It is shown in [42] that, the SA approach converges to the globally optimal solution almost surely if c is not lower than the depth of the deepest local optimum solution. In addition, the SA convergence for a continuous objective function was established in [43]. As shown in [43], if the state transition probability is far from zero on the predefined space and the temperature tends to zero, the SA method converges to the globally optimal solution in probability. Furthermore, if the cooling schedule $\{\mathrm{Tem}\,(k)\,|\forall k\}$ is reduced slowly enough as iteration $k \to \infty$, such that $\sum\limits_{k=1:\infty} \exp\left(-\dfrac{c}{\mathrm{Tem}\,(k)}\right) = \infty$ for $c > 0$, the global convergence is almost sure [44], since a slowly-decreasing temperature offers great opportunities for low-belief particles to exit from local optimal solutions.

B. Convergence Analysis of PASS

Unlike above methods, the PASS algorithm is defined on a compact set with a continuous objective function and driven by different particle transition and update schemes. To establish its convergence, we assume the proposed PASS algorithm satisfies the following conditions.

- C1. The state space $\mathscr{R}$ of the complete variable $\boldsymbol{\alpha}_R$ is a bounded closed subset of the Hilbert space $\mathbb{R}^6$.
- C2. The objective function $p(\mathbf{z}|\boldsymbol{\alpha}_R)$ is continuous on $\mathscr{R}$.
- C3. There exists at least one solution $\boldsymbol{\alpha}_R^\star$ in $\mathscr{R}$ such that the objective function $p(\mathbf{z}|\boldsymbol{\alpha}_R)$ reaches its maximal value

$\mathscr{P}^\star$ at $\boldsymbol{\alpha}_R^\star$, where $\mathscr{P}^\star = \sup\{p(\mathbf{z}|\boldsymbol{\alpha}_R) : \forall \boldsymbol{\alpha}_R \in \mathscr{R}\}$, and $\boldsymbol{\alpha}_R^\star = \arg\max_{\boldsymbol{\alpha}_R} p(\mathbf{z}|\boldsymbol{\alpha}_R)$.

- C4. The state transition probability $p\big(\boldsymbol{\alpha}_k^\flat(n)|\boldsymbol{\alpha}_k(n)\big)$ associated with candidate update state $\boldsymbol{\alpha}_k^\flat(n)$ from a search particle $\boldsymbol{\alpha}_k(n)$ is continuous and non-zero, $\forall n = 1 : N_S$.
- C5. The acceptance probability of a bad candidate update (where $\varphi_k(n) < \varphi_k^\flat(n)$) converges to zero almost surely, *i.e.*, $\Pr\Big\{\lim_{k\to\infty} \exp\Big(-\dfrac{\varphi_k(n) - \varphi_k^\flat(n)}{\mathcal{T}\left(\varphi_k(n)\right)} k\Big) = 0\Big\} = 1$.

Remark 4. Condition C4 means that the update sequence $\big\{\boldsymbol{\alpha}_k^\flat(n)|\forall k = 1 : K,\ K \to \infty\big\}$, $\forall n = 1 : N_S$, can visit every position in $\mathscr{R}$ with a certain probability after sufficient iterations. In addition, condition C5 implies an asymptotically decreasing acceptance probability of the worse candidate update so as to yield an upward-converging behaviour for a maximization issue, as will be addressed in Lemma 2. □

Definition 1 [Area of Attraction]. For a scalar $\varepsilon > 0$, the local area $\mathscr{L}_\varepsilon = \{\boldsymbol{\alpha}_R \in \mathscr{R} : \mathscr{P}^\star - p(\mathbf{z}|\boldsymbol{\alpha}_R) \le \varepsilon\}$ around the global optimal solution(s) $\boldsymbol{\alpha}_R^\star$ is said to be an *area of attraction* (AOA) if it satisfies $p(\mathbf{z}|\boldsymbol{\alpha}_R) \ge p(\mathbf{z}|\boldsymbol{\alpha}_R')\ \forall \boldsymbol{\alpha}_R \in \mathscr{L}_\varepsilon$, $\forall \boldsymbol{\alpha}_R' \notin \mathscr{L}_\varepsilon$, and there is no local optimum in $\mathscr{L}_\varepsilon$.

Lemma 1 [Existence of AOA]. Given conditions C1–C5, for a sufficiently small positive scalar $\varepsilon > 0$ and $\varepsilon \ll \varepsilon_U$, $\forall \varepsilon_U > 0$, there must exist an AOA $\mathscr{L}_\varepsilon = \{\boldsymbol{\alpha}_R \in \mathscr{R} : \mathscr{P}^\star - p(\mathbf{z}|\boldsymbol{\alpha}_R) \le \varepsilon\}$ around the globally optimal solution(s).

Proof: The proof is presented in APPENDIX A. ■

Remark 5. Lemma 1 indicates a mild condition that the objective function $p(\mathbf{z}|\boldsymbol{\alpha}_R)$ fluctuates slowly around $\mathscr{P}^\star$. It also indicates that the candidate update from a position out of AOA to a position in AOA is a good update with an increased belief, *i.e.*, $p(\mathbf{z}|\boldsymbol{\alpha}_k^\flat(n)) \ge p(\mathbf{z}|\boldsymbol{\alpha}_k(n))$, $\forall \boldsymbol{\alpha}_k(n) \notin \mathscr{L}_\varepsilon$, $\forall \boldsymbol{\alpha}_k^\flat(n) \in \mathscr{L}_\varepsilon$. Therefore, based on Eq. (25), this candidate update will must be accepted. Mathematically, its acceptance probability is one, *i.e.*, $p_{\mathrm{a}}\big\{\boldsymbol{\alpha}_{k+1}(n) = \boldsymbol{\alpha}_k^\flat(n) \in \mathscr{L}_\varepsilon | \boldsymbol{\alpha}_k(n) \notin \mathscr{L}_\varepsilon\big\} = 1$. This conclusion is useful for understanding the proof of the forthcoming Theorem 1. □

Lemma 2 [Upwards-Convergence Behavior]. The belief $\varphi_k(n)$ of each search particle $\boldsymbol{\alpha}_k(n)$ is upwards converging with sufficient iterations almost surely, *i.e.*, $\forall n = 1 : N_S$,

$$\lim_{k\to\infty} \Pr\big\{\varphi_{k+1}(n) \ge \varphi_k(n) : \forall \boldsymbol{\alpha}_{k+1}(n), \boldsymbol{\alpha}_k(n) \in \mathscr{R}\big\} = 1.$$

Proof: The proof is presented in APPENDIX B. ■

For convenience, in the following we use $\hat{\boldsymbol{\alpha}}_k(N_S)$ to denote the PASS-based estimate (see Eq. (30)) associated with the search particle size N_S, at the kth iteration.

Theorem 1 [Convergence of PASS to Global Optimum]. Given the sufficiently large number of iterations, the PASS-based estimate $\hat{\boldsymbol{\alpha}}_k(N_S)$ in Eq. (30) will converge in probability to the globally optimal solution $\boldsymbol{\alpha}_R^\star$, i.e.,

$$\lim_{\substack{N_S\to\infty,\\ k\to\infty}} \Pr\big\{\|\hat{\boldsymbol{\alpha}}_k(N_S) - \boldsymbol{\alpha}_R^\star\|_2 \le \varepsilon\big\} = 1,\ \forall \varepsilon > 0, \tag{31}$$

where $\|\cdot\|_2$ denotes the ℓ_2-norm on a vector.

Proof: The proof is presented in APPENDIX C. It mainly follows the ideas in [43], but it is more strict with non-ignorable modifications. For example, Lemma 1 is proved and then utilized to enhance the proof of Theorem 1. ■

For convenience, we employ $\hat{\boldsymbol{\alpha}}_k\big(N_S, |\Omega_R|\big)$ to denote the PASS-based estimate associated with the search particle set size N_S and the measurement set size $|\Omega_R|$, at the kth iteration.

Theorem 2 [Convergence of PASS to True Value]. Given a sufficient number of search particles and iterations for an unbiased SPAO system, the PASS-based estimate $\hat{\boldsymbol{\alpha}}_k(N_S, |\Omega_R|)$ will converge in probability to the true value $\boldsymbol{\alpha}_R$, asymptotically, with a large measurement sample limit,

$$\lim_{\substack{N_S\to\infty,\\ k\to\infty,\\ |\Omega_R|\to\infty}} \Pr\big\{\|\hat{\boldsymbol{\alpha}}_k\big(N_S, |\Omega_R|\big) - \boldsymbol{\alpha}_R\|_2 \le \varepsilon\big\} = 1,\ \forall \varepsilon > 0.$$

Proof: The proof is presented in APPENDIX D. ■

Remark 6. Theorem 2 implies that the estimation error will tend to zero asymptotically with an infinitely large measurement sample set, and in such a case the gap between the PASS-based estimate $\hat{\boldsymbol{\alpha}}_k$ and true value $\boldsymbol{\alpha}_R$ will tend to vanish. □

V. PERFORMANCE ANALYSIS

In this section, a closed-form VLC-based localization error bound is derived. Following that, the VLC-based localization performance will be analysed in terms of Fisher information.

A. Closed-Form CRLB

We first give the following two assumptions on the VLC-based localization system for ease of analysis.

- (Assumption 1). The measurement noise is independently and identically Gaussian distributed with zero-mean and a non-zero precision, i.e., $\epsilon_m \sim \mathcal{N}\big(\epsilon_m|0, \omega_m\big)$ with $\omega_m \ne 0$, $\forall m \in \Omega_R$.
- (Assumption 2). We consider the LOS-only case in the following CRLB analysis, i.e., $\varsigma_{\mathsf{nlos},m} = 0$, $\forall m \in \Omega_R$.

The first assumption on measurement noises is reasonable since (i) the Gaussian assumption renders a tractable system modeling and easy analysis; (ii) it complies with central limit theorem for large samples; and (iii) given a finite mean and variance of noises, the Gaussian distribution gives rise to the maximum entropy (i.e., it is the distribution with minimum restriction on noise uncertainties) [46], [47]. That means, Gaussian model has the lowest risk of noise modeling mismatch in entropy, if we only have the knowledge of mean and variance of noises. Thus, Gaussian assumption on measurement noises has been adopted by a large number of VLC localization papers, e.g., [4], [9], [25], [32]–[34]. The second assumption is imposed in order to easily characterize the information contribution of LOS signal to VLC localization.

Based on the above assumptions, the unbiased estimate error of $\boldsymbol{\alpha}_R$, where $\boldsymbol{\alpha}_R = \big[\mathbf{x}_R; \mathbf{u}_R\big]$, is bounded as follows, [48]

$$\mathbb{E}\{\|\hat{\boldsymbol{\alpha}}_R - \boldsymbol{\alpha}_R\|_2^2\} \ge \mathrm{trace}\big(\boldsymbol{\mathcal{B}}(\boldsymbol{\alpha}_R)\big), \tag{32}$$

$$\boldsymbol{\mathcal{B}}(\boldsymbol{\alpha}_R) = \big(\boldsymbol{\mathcal{I}}(\boldsymbol{\alpha}_R)\big)^{-1}, \tag{33}$$

where $\boldsymbol{\mathcal{B}}(\boldsymbol{\alpha}_R)$ denotes the CRLB of $\boldsymbol{\alpha}_R$, and $\boldsymbol{\mathcal{I}}(\boldsymbol{\alpha}_R)$ is the Fisher information matrix (FIM) that is defined as [48]

$$\boldsymbol{\mathcal{I}}(\boldsymbol{\alpha}_R) = -\,\mathbb{E}_{\mathbf{z}|\boldsymbol{\alpha}_R}\big\{\nabla_{\boldsymbol{\alpha}_R,\boldsymbol{\alpha}_R^\top} \ln p\left(\mathbf{z}|\boldsymbol{\alpha}_R\right)\big\}, \tag{34}$$

where $\nabla_{\boldsymbol{\alpha}_R,\boldsymbol{\alpha}_R^\top}(\bullet)$ is the second-order derivative w.r.t. $\boldsymbol{\alpha}_R$, and $p\left(\mathbf{z}|\boldsymbol{\alpha}_R\right)$ denotes the likelihood given in (8).

Proposition 1 [**Closed-Form CRLB**]. Based on [49], the CRLB $\boldsymbol{\mathcal{B}}(\boldsymbol{\alpha}_R)$ of the VLC-based SPAO error will be formulated in the following compact form,

$$\boldsymbol{\mathcal{B}}(\boldsymbol{\alpha}_R) = \Big(\sum_{m\in\Omega_R} \omega_m \mathbf{A}_m(\boldsymbol{\alpha}_R) \Big)^{-1}, \tag{35}$$

where $\mathbf{A}_m(\boldsymbol{\alpha}_R)$ is the resolution matrix, given by

$$\mathbf{A}_m(\boldsymbol{\alpha}_R) = (\Psi_R')^2 \begin{bmatrix} \frac{\boldsymbol{\Theta}_m(\mathbf{x}_R,\mathbf{x}_R)}{\rho_m^6} & \frac{\boldsymbol{\Theta}_m(\mathbf{x}_R,\mathbf{u}_R)}{\rho_m^5} \\ \frac{\boldsymbol{\Theta}_m(\mathbf{u}_R,\mathbf{x}_R)}{\rho_m^5} & \frac{\boldsymbol{\Theta}_m(\mathbf{u}_R,\mathbf{u}_R)}{\rho_m^4} \end{bmatrix}, \tag{36}$$

where $\boldsymbol{\Theta}_m(\boldsymbol{\alpha}_i,\boldsymbol{\alpha}_j)$, $\forall \boldsymbol{\alpha}_i,\boldsymbol{\alpha}_j \in \{\mathbf{x}_R,\mathbf{u}_R\}$, is given by

$$\boldsymbol{\Theta}_m(\mathbf{x}_R,\mathbf{x}_R) = \mathbb{E}\left\{\mathbf{K}_m \mathbf{s}_m \mathbf{s}_m^\top \mathbf{K}_m^\top\right\}, \tag{37}$$

$$\boldsymbol{\Theta}_m(\mathbf{x}_R,\mathbf{u}_R) = \mathbb{E}\left\{\mathbf{K}_m \mathbf{s}_m \mathbf{y}_m^\top \mathbf{V}_R^\top\right\}, \tag{38}$$

$$\boldsymbol{\Theta}_m(\mathbf{u}_R,\mathbf{x}_R) = \big(\boldsymbol{\Theta}_m(\mathbf{x}_R,\mathbf{u}_R)\big)^\top, \tag{39}$$

$$\boldsymbol{\Theta}_m(\mathbf{u}_R,\mathbf{u}_R) = \mathbb{E}\left\{\mathbf{V}_R \mathbf{F}_m \mathbf{V}_R^\top\right\}, \tag{40}$$

in which $\mathbf{K}_m = [\mathbf{e}_m,\, \mathbf{u}_R,\, \mathbf{v}_m]$, $\mathbf{V}_R = \mathbf{I}_3 - \mathbf{u}_R\mathbf{u}_R^\top$ and

$$\mathbf{s}_m = \begin{bmatrix} -(r+3)(r+1)\big(\mathbf{e}_m^\top \mathbf{v}_m\big)^r \mathbf{e}_m^\top \mathbf{u}_R \\ (r+1)\big(\mathbf{e}_m^\top \mathbf{v}_m\big)^r \\ r(r+1)\big(\mathbf{e}_m^\top \mathbf{v}_m\big)^{r-1} \mathbf{e}_m^\top \mathbf{u}_R \end{bmatrix}, \tag{41}$$

$$\mathbf{y}_m = (r+1)\left(\mathbf{e}_m^\top \mathbf{v}_m\right)^r \mathbf{e}_m, \tag{42}$$

$$\mathbf{F}_m = (r+1)^2\left(\mathbf{e}_m^\top \mathbf{v}_m\right)^{2r} \mathbf{e}_m \mathbf{e}_m^\top, \tag{43}$$

where $\mathbf{e}_m$ is given by (2), and ρ_m is transmission distance,

$$\rho_m = \|\mathbf{x}_R - \mathbf{p}_m\|_2. \tag{44}$$

Proof: The derivation is given in APPENDIX E. ∎

Remark 7. The resolution matrix $\mathbf{A}_m(\boldsymbol{\alpha}_R)$ indicates the capability to recognize the difference in variable $\boldsymbol{\alpha}_R$, for a given variation of measurement z_m [50], [51]. □

Remark 8. It is shown in (35) that the VLC-based SPAO performance depends on (I) the number of independent measurements, i.e., $|\Omega_R|$, (II) LED deployment $\{\mathbf{p}_m|\forall m \in \Omega_R\}$, (III) LED orientations $\{\mathbf{v}_m|\forall m \in \Omega_R\}$, (IV) measurement resolution $\{\mathbf{A}_m(\boldsymbol{\alpha}_R)|\forall m \in \Omega_R\}$, (V) prior knowledge of UE states and (VI) the measurement precision $\{\omega_m|\forall m \in \Omega_R\}$. In addition, the SPAO-based CRLB $\boldsymbol{\mathcal{B}}(\boldsymbol{\alpha}_R)$ scales with $|\Omega_R|$ as $\mathcal{O}(1/|\Omega_R|)$ [51]. □

B. Fisher Information Analysis

The FIM $\boldsymbol{\mathcal{I}}(\boldsymbol{\alpha}_R)$ quantifies the largest accuracy that VLC-based SPAO can achieve. Based on the obtained CRLB in (35), we shall study the VLC-based positioning and orientating performance limits, respectively, in terms of FIM analysis. The scaling of FIM w.r.t. transmission distance, incidence direction and measurement noise intensity will be revealed.

Given one measurement z_m, based on (35), the FIM contributed by this measurement is quantified as

$$\boldsymbol{\mathcal{I}}_m(\boldsymbol{\alpha}_R) = \omega_m \mathbf{A}_m(\boldsymbol{\alpha}_R), \tag{45}$$

where $\mathbf{A}_m(\boldsymbol{\alpha}_R)$ is given by Eq. (36). In addition, let γ_m denote the SNR associated with z_m, that is given by

$$\gamma_m = \mathbb{E}\{\omega_m (\Psi_R')^2\},\ \forall m \in \Omega_R. \tag{46}$$

Theorem 3 [Equivalent Positioning Information]. Equivalent positioning information (EPI) $\boldsymbol{\mathcal{I}}_m(\mathbf{x}_R)$ with respect to the mth LED transmitter is expressed as

$$\boldsymbol{\mathcal{I}}_m(\mathbf{x}_R) = \gamma_m \rho_m^{-6} \boldsymbol{\Theta}_m^\natural(\mathbf{x}_R),\ \forall m \in \Omega_R, \tag{47}$$

where $\boldsymbol{\Theta}_m^\natural(\mathbf{x}_R)$ denotes the direction information associated with UE positioning, given by (48) (on the top of next page), which only depends on the orientations $\mathbf{v}_m$, $\mathbf{u}_R$ and the incidence direction $\mathbf{e}_m$, but has nothing to do with the transmission distance ρ_m.

Proof: Based on Schur complement theory [52], Eq. (47) can be easily derived from Eq. (36). ∎

Remark 9. The EPI matrix $\boldsymbol{\mathcal{I}}_m(\mathbf{x}_R)$ presents the information of UE location estimate $\hat{\mathbf{x}}_R$ contributed by measurement z_m, which decays with six powers of the relative distance ρ_m. In addition, $\boldsymbol{\mathcal{I}}_m(\mathbf{x}_R)$ is linear with γ_m and $\boldsymbol{\Theta}_m^\natural(\mathbf{x}_R)$, where $\boldsymbol{\Theta}_m^\natural(\mathbf{x}_R)$ represents the associated information gained from transceiver orientations and incidence direction. □

Theorem 4 [Equivalent Orientating Information]. Equivalent orientating information (EOI) $\boldsymbol{\mathcal{I}}_m(\mathbf{u}_R)$ with respect to the mth LED transmitter is expressed as

$$\boldsymbol{\mathcal{I}}_m(\mathbf{u}_R) = \gamma_m \rho_m^{-4} \boldsymbol{\Theta}_m^\natural(\mathbf{u}_R),\ \forall m \in \Omega_R, \tag{49}$$

where the orientating-associated direction information matrix $\boldsymbol{\Theta}_m^\natural(\mathbf{u}_R)$ is given by (50) (on the top of next page), that depends on the orientations $\mathbf{v}_m$, $\mathbf{u}_R$ and the incidence direction $\mathbf{e}_m$ but which is unrelated to the transmission distance ρ_m.

Proof: Based on Schur complement theory [52], Eq. (49) can be easily derived from Eq. (36). ∎

Remark 10. The EOI matrix $\boldsymbol{\mathcal{I}}_m(\mathbf{u}_R)$ stands for the information of UE orientation estimate $\hat{\mathbf{u}}_R$ contributed by measurement z_m, which decays with four powers of transmission distance ρ_m. In addition, $\boldsymbol{\mathcal{I}}_m(\mathbf{u}_R)$ is linear with γ_m and $\boldsymbol{\Theta}_m^\natural(\mathbf{u}_R)$, where $\boldsymbol{\Theta}_m^\natural(\mathbf{u}_R)$ indicates the information contributed by transceiver orientations and the incidence direction. □

VI. NUMERICAL SIMULATION

In this section, simulation results are presented to examine the proposed PASS-based SPAO scheme for VLCs.

A. Simulation Settings

We consider the following parameter choices unless specified otherwise in subsection B. We consider $M = 81$ LEDs installed on the ceiling of a room with the size of $9[\mathrm{m}] \times 9[\mathrm{m}] \times 4[\mathrm{m}]$, and we assume they are uniformly distributed. In addition, we consider a common case that all LED orientations are downward, i.e., $\mathbf{v}_m = [0,0,-1]^\top$, $\forall m = 1:M$, although the proposed algorithm has no special requirements on LED orientations. The UE appears in the room at a random location and with a random orientation. In addition, we have the following settings of system parameters throughout this simulation, i.e., $\Psi_R = 1\,[\mathrm{cm}^2]$, $r = 1$, $W_T = 2.2\,[\mathrm{Watt}]$, $G_R = 1$, $\Gamma_R = 2.25$, $\theta_{\mathrm{FOV}} = \phi_{\mathrm{FOV}} = \pi/2$, and SNR

$$\mathbf{\Theta}_m^{\natural}(\mathbf{x}_R) = \mathbf{\Theta}_m(\mathbf{x}_R, \mathbf{x}_R) - \mathbf{\Theta}_m(\mathbf{x}_R, \mathbf{u}_R)\big(\mathbf{\Theta}_m(\mathbf{u}_R, \mathbf{u}_R)\big)^{-1}\mathbf{\Theta}_m(\mathbf{u}_R, \mathbf{x}_R). \tag{48}$$

$$\mathbf{\Theta}_m^{\natural}(\mathbf{u}_R) = \mathbf{\Theta}_m(\mathbf{u}_R, \mathbf{u}_R) - \mathbf{\Theta}_m(\mathbf{u}_R, \mathbf{x}_R)\big(\mathbf{\Theta}_m(\mathbf{x}_R, \mathbf{x}_R)\big)^{-1}\mathbf{\Theta}_m(\mathbf{x}_R, \mathbf{u}_R). \tag{50}$$

$\gamma_m = 20$[dB], unless specified otherwise, $\forall m = 1 : M$. These settings follow from a typical LED setup that are widely adopted in papers such as [9], [16], [32]. Let η_{nlos} denote the percentage of NLOS signal power over the total received signal power. For a given $\eta_{\text{nlos}} \in [0, 1]$, we set the NLOS signal component in (1) to be $\varsigma_{\mathsf{nlos},m} = \dfrac{\eta_{\text{nlos}}}{1-\eta_{\text{nlos}}} h_m\big(\mathbf{x}_R, \mathbf{u}_R\big)\,\mathsf{rand}$, $\forall m \in \Omega_R$, where rand denotes a random number in [0,1]. In the following section VI-B-1, 2 and 4 we set $\eta_{\text{nlos}} = 0$, and in section VI-B-3 we set $\eta_{\text{nlos}} \in [0.1, 0.5]$ to study the effect of NLOS signal strength on VLC localization performance, unless specified otherwise.

In simulations, we consider the following algorithms as localization baseline methods for comparison.

- (Baseline 1) Geometric trilateration algorithm [14] with perfect alignment of LED and UE orientation angles;
- (Baseline 2) Brute force search (BFS)-assisted maximum likelihood estimate (MLE) algorithm;
- (Baseline 3) Newton-Raphson positioning (NRP) method [9] using locally linear approximation for nonlinear system model;
- (Baseline 4) Traditional PSO method [22] dedicated to non-convex optimization;
- (Baseline 5) Traditional SA method [25] dedicated to non-convex optimization.

In the proposed PASS algorithm, we use $N_D = 9$ detection particles for each search particle, and a total of $N_S = 20$ search particles are used. For a fair comparison, the search particle set sizes of PSO and SA are set to be $N_S = 200$ and 140, respectively, in simulations. The associated parameter settings are summarized in Table I.

TABLE I
PARAMETER SETTINGS

Algorithm	Parameter Settings
The proposed PASS	$\lambda_0 = 0.1$, $\lambda_1 = 0.4$, $\lambda_2 = 0.6$, $L_0 = 0.8$, $N_S = 20$, $N_D = 9$, $c_1 = 2$, $c_2 = 0.1$.
Trad. PSO [22]	$N_S = 200$, $K = 50$, $\lambda_0 = 0.2$, $\lambda_1 = 1.8\mathsf{rand}$, $\lambda_3 = 0.9\mathsf{rand}^{\dagger}$.
Trad. SA [25]	$N_S = 140$, $K = 50$, $\text{Tem} = 0.5^{\ddagger}$.
BFS-aided MLE	$N_{\mathsf{search}} = 50^{*}$.

$^{\dagger}\lambda_3$ is the acceleration factor of PSO algorithm for the personal best knowledge-related update.
‡We assume that $p_{\text{a}} = \exp\big(-\text{Tem}\,k\big)$ when $\varphi_k^{\flat}(t) < \varphi_k(t)$.
$^{*}N_{\mathsf{search}}$ is the number of trial grid samples at each dimension of parameter space, which is set to be 50 so as to preserve a proper resolution in parameter spaces. Note that $(\mathbf{x}_R, \mathbf{u}_R) \in \mathbb{R}^6$.

B. Simulation Results

In the following, we will first present the overall localization errors (averaged over different UE locations, orientations and LED locations) of the proposed PASS algorithm and various baseline approaches mentioned above. Then, we will assess the PASS algorithm in various scenarios associated with diverse UE location, UE orientation, the height of UE, SNR and the number of LEDs, respectively.

1) Overall Performance: The convergence of achieved positioning and orientating errors are presented in Figs. 4 and 5, respectively. The cumulative distribution functions (CDFs) of positioning and orientating errors are presented in Figs. 6 and 7, respectively.[4] We can see from Figs. 4 and 5 that, the proposed PASS algorithm can achieve a sub-linear convergence rate which is comparable to that of conventional PSO and SA methods, and at the meanwhile it can achieve a lower stationary error than PSO and SA methods due to the efficient particle update rule design in our PASS algorithm. Specifically, when SNR is 20 [dB], the overall positioning error of the PASS algorithm is 0.1[m], and the overall orientating error is 0.07[m] (corresponding to an angle error of 5 [deg]). In addition, it is shown in Fig. 4 and 6 that the PASS algorithm can achieve positioning and orientating errors closer to CRLBs. Thus, PASS outperforms existing approaches (NRP, Trilateration, PSO and SA) under the same parameter settings,[5] due to the benefits from multi-scale search scheme that explores diverse update knowledge. Since NRP and Trilateration are prone to be trapped into local optima of the non-convex SPAO problem, when this local optimum is far away from the global optimum, the localization errors will be large. Besides, due to the limited knowledge for particle update, the PSO and SA-based localization errors are also larger than PASS.

2) Algorithm Complexities: The theoretical computational complexities and practically consumed CPU time of various VLC localization methods are summarized in Table II. It is shown that the proposed PASS algorithm is slightly larger in consumed CPU time than NRP and trilateration methods in a computationally affordable level. However, it is comparable to NRP, PSO and SA methods. Particularly, it is much smaller than BSF-aided MLE algorithm in consumed CPU time. Overall, the proposed SSVBI algorithm can provide a satisfactory VLC localization solution (with near-CRLB accuracy) in an affordable computational cost.

[4]Note that, NRP and Trilateration methods cannot obtain UE orientation estimate. Thus, no orientating result of them is considered in Fig. 5 and 7.

[5]Note that, in the BFS-aided MLE algorithm, $N_{\mathsf{search}} = 100$, which gives rise to a location resolution of 9[m]/50 = 0.18[m]. However, the CPU time it consumes is computational unaffordable (larger than 10^5[s]) as will be shown in Table II. Thus, in Fig. 6 we exclude its localization result.

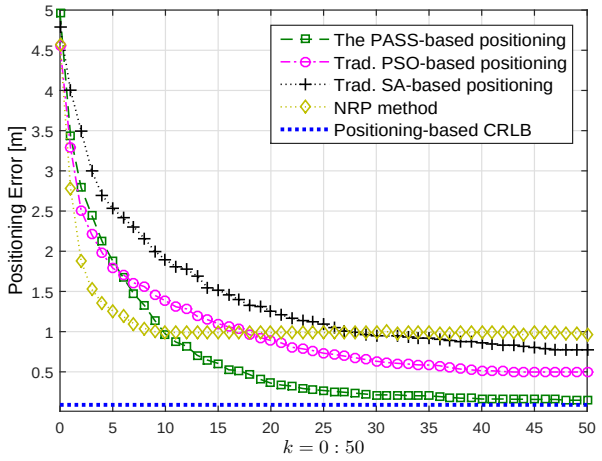

Fig. 4. The convergence of positioning errors $\|\hat{\mathbf{x}}_R - \mathbf{x}_R\|_2$ (SNR $= 20$dB).

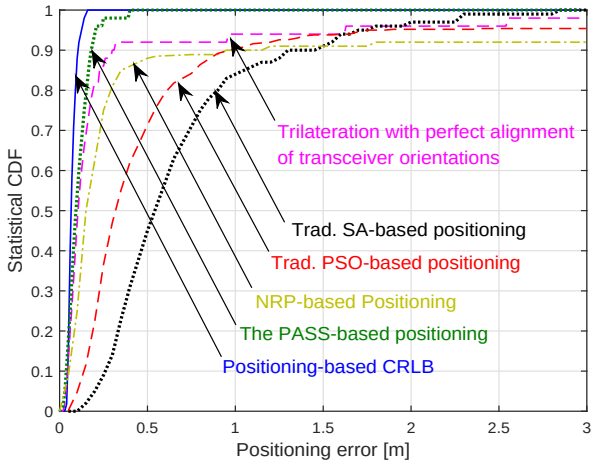

Fig. 6. The cumulative distributions of positioning errors [m] (SNR $= 20$dB).

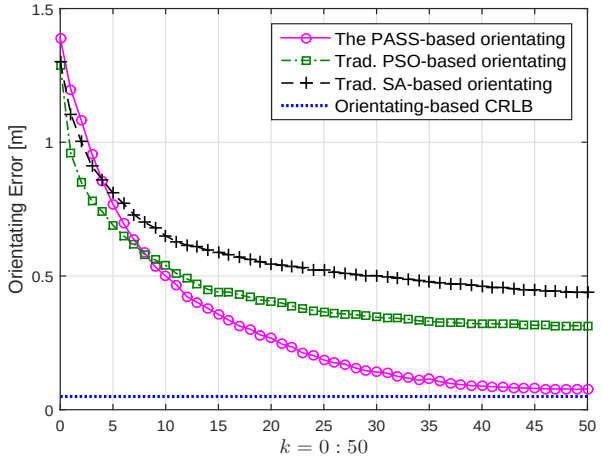

Fig. 5. The convergence of orientation errors $\|\hat{\mathbf{u}}_R - \mathbf{u}_R\|_2$ (SNR $= 20$dB).

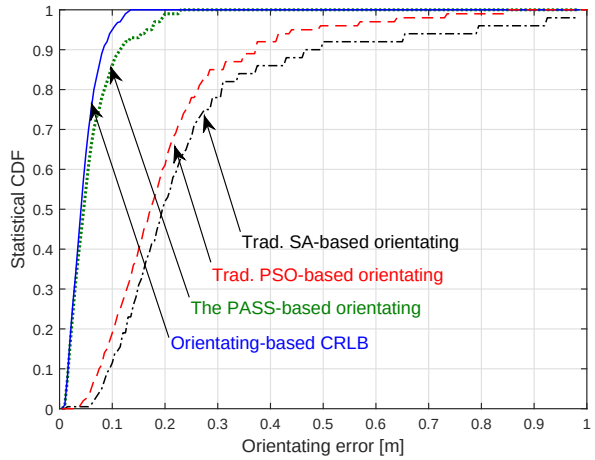

Fig. 7. The cumulative distributions of orientation errors [m] (SNR $= 20$dB).

TABLE II
COMPUTATIONAL COMPLEXITIES

Algorithm	Theoretical complexity	CPU time
The proposed PASS	$\mathcal{O}\big(N_S N_D \lvert\Omega_R\rvert K\big)^\dagger$	**2.16**[s]
Trad. PSO	$\mathcal{O}\big(N_S \lvert\Omega_R\rvert K\big)^\dagger$	2.58[s]
Trad. SA	$\mathcal{O}\big(N_S \lvert\Omega_R\rvert K\big)^\dagger$	2.42[s]
Trilateration	$\mathcal{O}\big(\lvert\Omega_R\rvert\big)$	0.09[s]
NRP method	$\mathcal{O}\big(\lvert\Omega_R\rvert K\big)$	0.47[s]
BFS-aided MLE	$\mathcal{O}\big(N_{\text{search}}^6 \lvert\Omega_R\rvert\big)^\ddagger$	129437.87[s]

†Note that we have set $N_S = 20$, 200 and 140 for PASS, PSO and SA algorithm, respectively, to ensure these three algorithms a comparable localization resolution. If we set the same $N_S = 20$ for PSO and SA as the proposed PASS algorithm, the consumed CPU time of PSO and SA will be 0.59[s] and 0.46[s], respectively. Then, the proposed PASS algorithm will be slightly larger in CPU time than PSO and SA in a computationally affordable level. But in this case the localization performance of PSO and SA will become very poorer than the proposed PASS algorithm.
‡Note that $N_{\text{search}} = 50$ trial grids in each dimension of parameter space $(\mathbf{x}_R, \mathbf{u}_R) \in \mathbb{R}^6$ are used for a satisfactory resolution.

3) Impact of SNR and NLOS Signals: We assess the performance of the PASS algorithm when SNR is within 0 to 60[dB]. Both LOS and non-line-of-light (NLOS) cases are considered. We can see from Fig. 8 that, the PASS-based positioning error can be as low as 0.002[m] when the SNR approaches a typical value of 60dB in VLCs [7], when only LOS presents. In addition, within the high SNR region, NLOS component will become the dominant error source that affects the VLC localization performance. If the NLOS component carries 10% of total received power [5], [40], there will be an error floor of 0.1[m], as shown in Fig. 8. Moreover, the UE location and orientation estimate errors of the proposed PASS algorithm under various NLOS power settings are given in Fig. 9, where the power of NLOS signals over the total power of received signals ranges from 0% to 40% and the SNR is fixed at 20[dB]. As we expected, a larger NLOS power leads to a larger localization error, and it shows a linear increasing of localization error with the NLOS signal strength.

4) Impact of Location, Orientation and Height of UE: The localization errors achieved by the PASS algorithm associated with various locations, orientations and heights of UE are presented in Fig. 10–13, respectively. As shown in Fig. 10, the inner region of room yields low localization errors. In addition, an upwards orientation of UE leads to a lower localization error as shown in Fig. 12, since in this case the

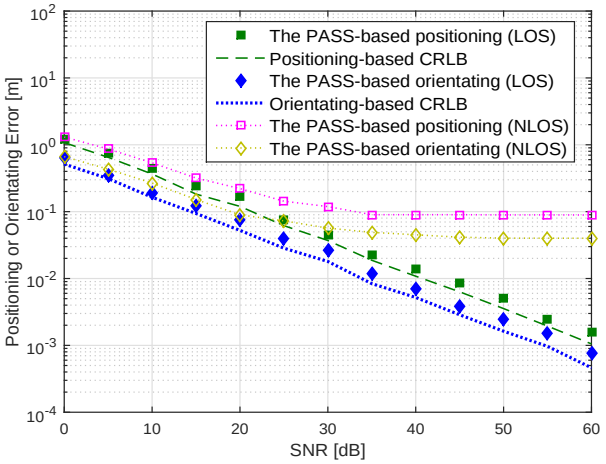

Fig. 8. The impact of SNR and diffuse signals on localization errors [m].

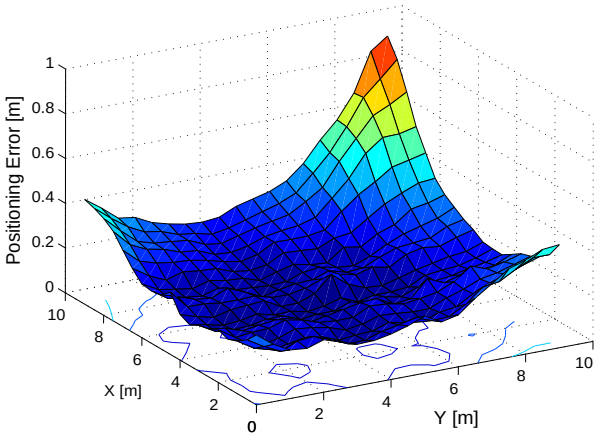

Fig. 10. The PASS-based positioning errors associated with various UE locations, where the height of UE is 1[m] and SNR is 20dB.

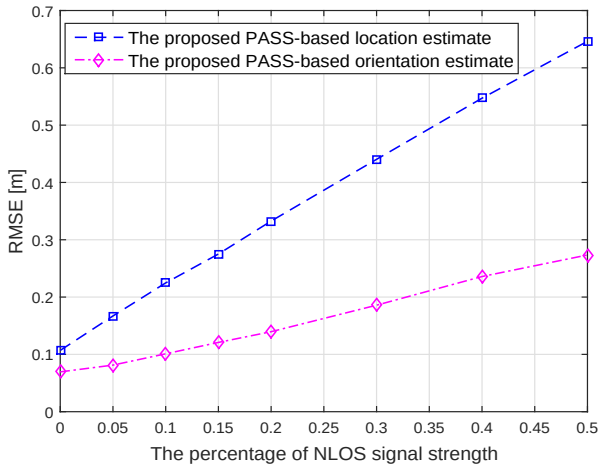

Fig. 9. The achieved location and orientation estimate errors of the proposed PASS algorithm v.s. the percentage of NLOS signal power.

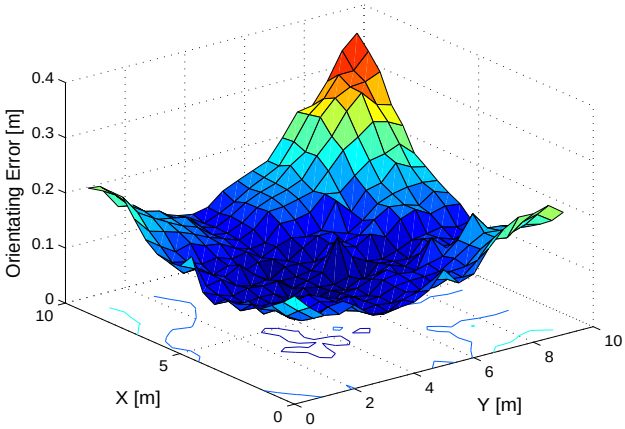

Fig. 11. The proposed PASS-based orientating errors associated with various UE locations, where the height of UE is 1[m] and SNR is 20dB.

UE orientation is more likely to align with LED orientations. In Fig. 13, it is shown that the UE height lower than 3[m] will yield a satisfactory localization performance for a 4[m]-high room. Moreover, we can see from Fig. 10 and 11 that the localization error will be slightly increased when the UE is near wall. This is mainly because the number of active LEDs will be reduced due to the limited FOV of UE. Also, from the perspective of localization error bound or Fisher information (see Section IV-B), the localization information will be reduced due to the poor geometric location relationship (i.e., the relative position, relative direction and orientation angle) between UE and LED arrays. This is because the relative geometric location relationship will essentially affect the equivalent SNR. Thus, the location close to wall will give rise to a poor VLC localization performance for UE.

5) Impact of the Number of LEDs: The PASS-based localization error associated with various numbers of LEDs are presented in Fig. 14. Note that, since the number of on-ceiling LEDs will not affect the NLOS effect in practice, we set the NLOS signal strength is fixed, i.e., $\eta_{\text{nlos}} = 0.1$ [5] for different settings of the number of LEDs. As shown, a larger number of LEDs will yield a lower localization error as expected. Meanwhile, it is found that 25 LEDs are enough for achieving a positioning error below 1.04 [m] (when SNR = 20dB). When $M > 25$, the marginal benefit reduces significantly, and the NLOS effect will become dominant error source.

VII. CONCLUSIONS

In this paper, we have studied the visible light RSS-based simultaneous portioning and orientating (SPAO) problem for UE of VLCs, which is of great challenge due to its non-convex problem nature resulted from the nonlinear RSS model w.r.t. UE location parameters. Hence, a novel multi-scale PASS algorithm with problem-specific update rule design is proposed to solve the non-convex SPAO problem. To be specific, the proposed PASS algorithm explores diverse update knowledge (i.e., (I) the global information, (II) the local information and (III) the historical information) to handle the non-convex optimization problem, thus improving the evolution efficiency. It has been established by convergence analysis that the proposed PASS algorithm can converge in probability to the globally

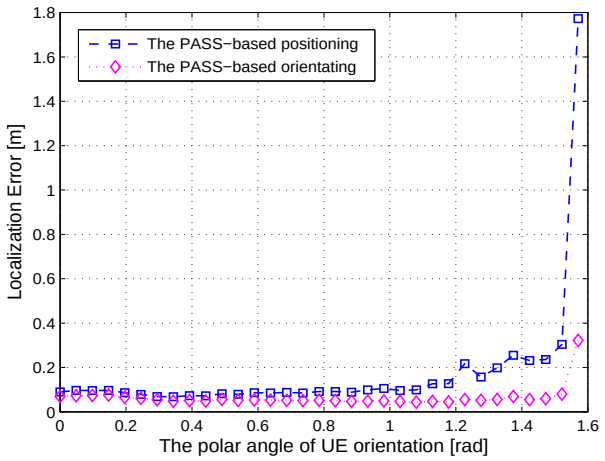

Fig. 12. The impact of UE orientation angle (polar angle) on the PASS-based localization errors, where the azimuthal angle of UE orientation is at random and SNR = 20dB.

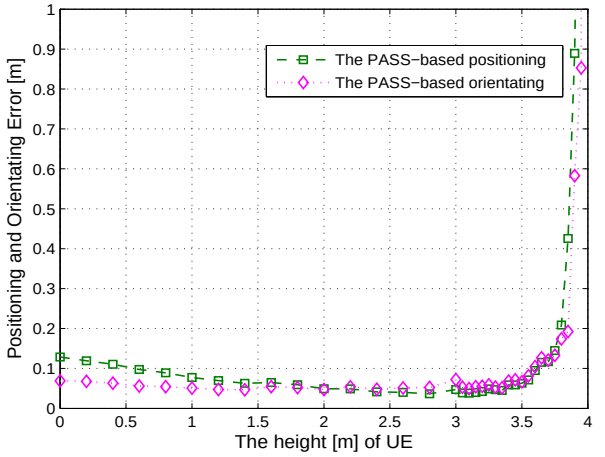

Fig. 13. The impact of UE height on the PASS-based localization errors, where we set SNR = 20dB.

optimal solution of the associated non-convex optimization problem, which is superior to conventional gradient-based methods that only ensure the convergence to local optima.

In addition, unlike the existing VLC-based positioning solution, the proposed PASS-based SPAO solution for VLCs does not require the knowledge of the height of UE or the perfect alignment of transceiver orientations. Thus, it is very desirable for practical VLC localization. Simulation results show that the proposed PASS algorithm provides an effective solution to the VLC-based SPAO problem.

Furthermore, a closed-form performance analysis is conducted to reveal the performance limits of the VLC-based SPAO. It is shown that the UE position and orientation accuracies are linear w.r.t. SNR and direction information. In addition, the position and orientation accuracies decay with six and four powers of the transmission distance, respectively.

Appendix A
The Proof of Lemma 1

Let $\mathscr{P}_\jmath^\natural$ denote the objective function value $p(\mathbf{z}|\boldsymbol{\alpha}_R^\natural)$ of the $\jmath$th locally optimal solution $\boldsymbol{\alpha}_\jmath^\natural \in \mathscr{R}$, $\forall \jmath = 1 : M_L$, where

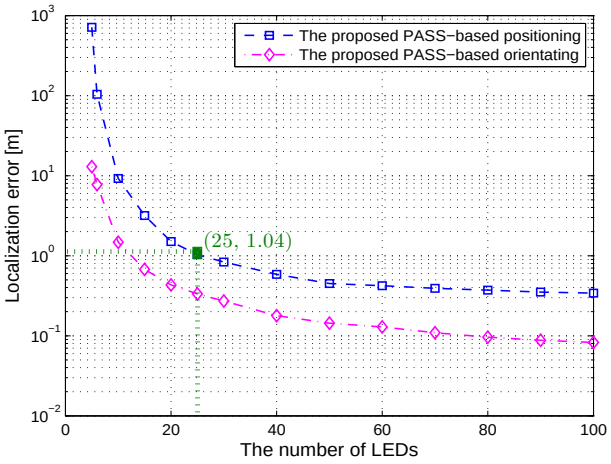

Fig. 14. The impact of the number of LEDs on localization performance, where we set SNR = 20dB.

the number of locally optimal solutions is assumed to be M_L. Let $\mathscr{P}^\sharp = \sup\{\mathscr{P}_\jmath^\natural | \forall \jmath = 1 : M_L\}$. Thus, $\mathscr{P}^\sharp < \mathscr{P}^\star$, which means that there is a non-ignorable gap between the global optimum value $\mathscr{P}^\star$ and the maximum of the locally optimum values, *i.e.*, $\mathscr{P}^\sharp$. That is to say, there exists a positive scalar $\varepsilon > 0$ such that $\mathscr{P}^\star - \mathscr{P}^\sharp > \varepsilon$.

Recall $\mathscr{L}_\varepsilon = \{\boldsymbol{\alpha}_R \in \mathscr{R} : p(\mathbf{z}|\boldsymbol{\alpha}_R) \geq \mathscr{P}^\star - \varepsilon\}$. Since $\mathscr{P}^\star - \varepsilon > \mathscr{P}^\sharp$, we have $p(\mathbf{z}|\boldsymbol{\alpha}_R) \geq p(\mathbf{z}|\boldsymbol{\alpha}'_R)$, $\forall \boldsymbol{\alpha}_R \in \mathscr{L}_\varepsilon$ and $\forall \boldsymbol{\alpha}'_R \notin \mathscr{L}_\varepsilon$ (i.e., $p(\mathbf{z}|\boldsymbol{\alpha}_R)$ is pseudo-convex in $\boldsymbol{\alpha}_R \in \mathscr{L}_\varepsilon$). Since $p(\mathbf{z}|\boldsymbol{\alpha}_R)$ is uniformly continuous on $\mathscr{R}$, thus $\|\boldsymbol{\alpha}_R - \boldsymbol{\alpha}_R^\star\|_2 < \delta$ holds, $\forall \boldsymbol{\alpha}_R \in \mathscr{L}_\varepsilon$, for two upper-bounded scalars $\varepsilon > 0$ and $\delta > 0$, if $p(\mathbf{z}|\boldsymbol{\alpha}_R) - \mathscr{P}^\star < \varepsilon$. Thus, there must exist an AOA $\mathscr{L}_\varepsilon$ without any local optimum point such that the objective function value of each point in this AOA is not lower than the value of any point outside this AOA.

Appendix B
The Proof of Lemma 2

The acceptance probability p_a of $\boldsymbol{\alpha}_k^\flat(n)$ can be reformulated as $p_\mathrm{a} = \min\left\{1, \exp\left(-\dfrac{\varphi_k(n) - \varphi_k^\flat(n)}{\mathcal{T}(\varphi_k(n))}k\right)\right\}$. Then, when the iteration number k approaches infinity, p_a follows that

$$\lim_{k\to\infty} p_\mathrm{a} = \begin{cases} 0, & \text{if } \varphi_k(n) < \varphi_k^\flat(n), \\ 1, & \text{if } \varphi_k(n) \geq \varphi_k^\flat(n). \end{cases} \tag{51}$$

Thus, the acceptance probability of a bad update will approach zero as iterations, while a good update will be approved directly. Thus, the probability of search particle being updated with an unreduced belief is cast as

$$\begin{aligned} &\Pr\{\varphi_{k+1}(n) \geq \varphi_k(n) : \forall \boldsymbol{\alpha}_{k+1}(n), \boldsymbol{\alpha}_k(n) \in \mathscr{R}\} \\ &= 1 - p_\mathrm{a}\{\varphi_k(n) < \varphi_k^\flat(n) : \forall \boldsymbol{\alpha}_{k+1}(n), \boldsymbol{\alpha}_k(n) \in \mathscr{R}\}. \end{aligned} \tag{52}$$

Combing Eqs. (52) and (51), Lemma 2 is proved.

Appendix C
The Proof of Theorem 1

This proof consists of two parts. The first is to address the probability of a better event that the search particle sequence

$\{\boldsymbol{\alpha}_{k+1}(n)|\forall k=1:K,\forall n=1:N_S\}$ hits the AOA $\mathscr{L}_\varepsilon$ from any initial states $\{\boldsymbol{\alpha}_1(n)|\forall t=1:N_S\}$ in $\mathscr{R}$. The second is to formulate the probability of a worse event that all of search particles in AOA $\mathscr{L}_\varepsilon$ escape out of the AOA.

1) The Probability of Better Event: Let's first revisit some definitions. Let $\mathscr{P}^\star=\sup\{p(\mathbf{z}|\boldsymbol{\alpha}_R):\forall\boldsymbol{\alpha}_R\in\mathscr{R}\}$ be the maximum value of $p(\mathbf{z}|\boldsymbol{\alpha}_R)$ on $\mathscr{R}$. Let $\mathscr{R}^\star$ denote the set of states that maximize $p(\mathbf{z}|\boldsymbol{\alpha}_R)$, *i.e.*, $\mathscr{R}^\star=\{\boldsymbol{\alpha}_R:p(\mathbf{z}|\boldsymbol{\alpha}_R)=\mathscr{P}^\star\}$. Then, the globally optimal solution $\boldsymbol{\alpha}_R^\star$ is in $\mathscr{R}^\star$. For a certain scalar $\varepsilon>0$, let $\mathscr{L}_\varepsilon=\{\boldsymbol{\alpha}_R\in\mathscr{R}:p(\mathbf{z}|\boldsymbol{\alpha}_R)\geq\mathscr{P}^\star-\varepsilon\}$ be an AOA around $\mathscr{R}^\star$ that is defined in Definition 1. Based on Lemma 1, there must exist an AOA $\mathscr{L}_\varepsilon$ around $\mathscr{R}^\star$ for the VLC-based SPAO issue considered in this paper.

Let $\varrho=\inf\big\{p\big(\boldsymbol{\alpha}_k^\flat(n)|\boldsymbol{\alpha}_k(n)\big):\forall\boldsymbol{\alpha}_k(n),\boldsymbol{\alpha}_k^\flat(n)\in\mathscr{R}\big\}$ be the minimum value of the transition probability from $\boldsymbol{\alpha}_k(n)$ to $\boldsymbol{\alpha}_k^\flat(n)$. Based on condition C4, $p\big(\boldsymbol{\alpha}_k^\flat(n)|\boldsymbol{\alpha}_k(n)\big)$ is nonzero, we thus have $\varrho>0$. Then, the probability $\kappa(\mathscr{L}_\varepsilon)$ of the candidate update state $\boldsymbol{\alpha}_k^\flat(n)$ visiting $\mathscr{L}_\varepsilon$ follows (53), where $p\big(\boldsymbol{\alpha}_k(n)\big)$ denotes the prior probability density function of $\boldsymbol{\alpha}_k(n)$, which is positively and finitely valued.

Since $\boldsymbol{\alpha}_k^\flat(n)\in\mathscr{L}_\varepsilon$ from $\boldsymbol{\alpha}_k(n)\notin\mathscr{L}_\varepsilon$ is a good update, *i.e.*, $p(\mathbf{z}|\boldsymbol{\alpha}_k^\flat(n))\geq p(\mathbf{z}|\boldsymbol{\alpha}_k(n))$, the acceptance probability is $p_{\rm a}\{\boldsymbol{\alpha}_{k+1}(n)=\boldsymbol{\alpha}_k^\flat(n):p(\mathbf{z}|\boldsymbol{\alpha}_k^\flat(n))\geq p(\mathbf{z}|\boldsymbol{\alpha}_k(n))\}=1$. Thus, the probability of search particle $\boldsymbol{\alpha}_{k+1}(n)$ being updated as $\boldsymbol{\alpha}_k^\flat(n)$ in $\mathscr{L}_\varepsilon$ is cast as the product of the visiting probability and acceptance probability,

$$\Pr\{\boldsymbol{\alpha}_{k+1}(n)=\boldsymbol{\alpha}_k^\flat(n)\in\mathscr{L}_\varepsilon\}=\kappa(\mathscr{L}_\varepsilon)p_{\rm a}=\kappa(\mathscr{L}_\varepsilon).\quad(54)$$

Based on Eq. (53) we know that $\kappa(\mathscr{L}_\varepsilon)\geq\iota(\mathscr{L}_\varepsilon)>0$, *i.e.*, the probability $\kappa(\mathscr{L}_\varepsilon)$ is lower bounded away from 0, thus so is $\Pr\{\boldsymbol{\alpha}_{k+1}(n)\in\mathscr{L}_\varepsilon\}$. Hence, the probability that none of $\{\boldsymbol{\alpha}_{k+1}(n)|\forall k=1:K\}$ visits $\mathscr{L}_\varepsilon$ is $\Pr\{\boldsymbol{\alpha}_{k+1}(n)\notin\mathscr{L}_\varepsilon|\forall k=1:K\}\leq\big(1-\iota(\mathscr{L}_\varepsilon)\big)^K$. For some constant $\delta>0$ and $\delta\ll1$, there exists a sufficiently large iteration number K_0 such that $\big(1-\iota(\mathscr{L}_\varepsilon)\big)^{K_0}\leq\delta$. Thus, we further have

$$\Pr\{\boldsymbol{\alpha}_{k+1}(n)\notin\mathscr{L}_\varepsilon|\forall k=1:K\}\leq\delta,\ \forall K\geq K_0.\quad(55)$$

As such, the probability that none of update sequences of all search particles visits $\mathscr{L}_\varepsilon$ follows $\Pr\{\boldsymbol{\alpha}_{k+1}(n)\notin\mathscr{L}_\varepsilon|\forall k=1:K,\forall n=1:N_S\}\leq\delta^{N_S}$. Thus, there must exist a sufficiently large number K_0 such that $\lim\limits_{N_S\to\infty}\Pr\{\boldsymbol{\alpha}_{k+1}(n)\notin\mathscr{L}_\varepsilon|\forall k=1:K,\ \forall n=1:N_S\}=0$, when $K\geq K_0$. Thus, we have

$$\lim_{\substack{K\to\infty,\\N_S\to\infty}}\Pr\{\boldsymbol{\alpha}_{k+1}(n)\in\mathscr{L}_\varepsilon|\forall k=1:K,\ \forall n=1:N_S\}=1.\quad(56)$$

This means, after sufficient iterations, there must be at least one search particle hitting the local area $\mathscr{L}_\varepsilon$ around the global optimum solution, regardless of its initial state.

2) The Probability of Worse Event: Let $\mathcal{E}_k(n)$ be a worse event of search particle $\boldsymbol{\alpha}_k(n)$ at the kth iteration that $\boldsymbol{\alpha}_{k+1}(n)$ escapes out of $\mathscr{L}_\varepsilon$ from $\boldsymbol{\alpha}_k(n)\in\mathscr{L}_\varepsilon$, with a reduced belief, *i.e.*, $p\big(\mathbf{z}|\boldsymbol{\alpha}_{k+1}(t)\big)\leq p\big(\mathbf{z}|\boldsymbol{\alpha}_k(n)\big)$. In short, $\mathcal{E}_k(n)=\big\{\boldsymbol{\alpha}_k^\flat(n)\notin\mathscr{L}_\varepsilon,\boldsymbol{\alpha}_k(n)\in\mathscr{L}_\varepsilon|p\big(\mathbf{z}|\boldsymbol{\alpha}_{k+1}(n)\big)\leq p\big(\mathbf{z}|\boldsymbol{\alpha}_k(n)\big)\big\}$.

Let $\widetilde{\varphi}_k(n)=\varphi_k(n)-\varphi_k^\flat(n)$ be the difference between the beliefs $\varphi_k(n)$ and $\varphi_k^\flat(n)$ of candidate update $\boldsymbol{\alpha}_k^\flat(n)\notin\mathscr{L}_\varepsilon$ and its previous state $\boldsymbol{\alpha}_k(n)\in\mathscr{L}_\varepsilon$, respectively. For a worse event with a reduced belief, we know $\widetilde{\varphi}_k(n)>0$, and there is a constant $\delta>0$ such that $\widetilde{\varphi}_k(n)>\delta$. In this case we have

$$\exp\bigg(-\frac{\varphi_k(n)-\varphi_k^\flat(n)}{\mathcal{T}\left(\varphi_k(n)\right)}k\bigg)\leq\exp\bigg(-\frac{\delta}{\mathcal{T}_\star}k\bigg),\quad(57)$$

where $\mathcal{T}_\star=\sup\big\{\mathcal{T}\left(\varphi_k(n)\right):\forall\boldsymbol{\alpha}_k(n)\in\mathscr{R}\big\}$ is the maximum value of temperature function $\mathcal{T}\left(\varphi_k(n)\right)$ on $\mathscr{R}$, and $\mathcal{T}\left(\varphi_k(n)\right)$ is given by Eq. (27). In addition, based on condition C5, there exists a sufficiently large iteration number K_0 such that $\exp\left(-\frac{\delta}{\mathcal{T}_\star}k\right)$ is lower than a finite positive constant $\varepsilon_{K_0}\ll1$. In other words, for some $\varepsilon_{K_0}\in(0,1)$, $\exp\left(-\frac{\delta}{\mathcal{T}_\star}k\right)\leq\varepsilon_{K_0}$ holds $\forall k\geq K_0$. Hence, the acceptance probability of personal worse event $\mathcal{E}_k(n)$ follows $p_{\rm a}\big\{\mathcal{E}_k(n)\big\}\leq\exp\left(-\frac{\delta}{\mathcal{T}_\star}k\right)\leq\varepsilon_{K_0},\ \forall k\geq K_0$.

Suppose the appearing probability of a personal worse event is $\kappa'(\mathscr{L}_\varepsilon^{\rm C})$, which is given by

$$\kappa'(\mathscr{L}_\varepsilon^{\rm C})=\iint\limits_{\substack{\boldsymbol{\alpha}_k(n)\in\mathscr{L}_\varepsilon,\\\boldsymbol{\alpha}_k^\flat(n)\in\mathscr{L}_\varepsilon^{\rm C}}}p\big(\boldsymbol{\alpha}_k^\flat(n)|\boldsymbol{\alpha}_k(n)\big)p\big(\boldsymbol{\alpha}_k(n)\big)\,{\rm d}\boldsymbol{\alpha}_k(n){\rm d}\boldsymbol{\alpha}_k^\flat(n),$$

where $p\big(\boldsymbol{\alpha}_k(n)\big)$ is the prior probability of $\boldsymbol{\alpha}_k(n)$, and $\mathscr{L}_\varepsilon^{\rm C}$ is the complementary set of $\mathscr{L}_\varepsilon$ over $\mathscr{R}$, *i.e.*, $\mathscr{L}_\varepsilon^{\rm C}=\mathscr{R}\setminus\mathscr{L}_\varepsilon$, and the symbol $\setminus$ denotes the set minus.

Thus, the probability of $\boldsymbol{\alpha}_{k+1}(n)$ escapeing out of $\mathscr{L}_\varepsilon$ from $\boldsymbol{\alpha}_k(n)\in\mathscr{L}_\varepsilon$ is $\Pr\{\mathcal{E}_k(n)\}=\kappa'(\mathscr{L}_\varepsilon^{\rm C})p_{\rm a}\{\mathcal{E}_k(n)\}$. Since $\kappa'(\mathscr{L}_\varepsilon^{\rm C})$ is bounded from above, the probability that all updated states $\{\boldsymbol{\alpha}_{k+1}(n)\notin\mathscr{L}_\varepsilon|\forall n=1:N_S\}$ escape from $\mathscr{L}_\varepsilon$ at the $(k+1)$th iteration follows $\lim\limits_{N_S\to\infty}\Pr\big\{\mathcal{E}_k(n)|\forall n=1:N_S\big\}\leq\lim\limits_{N_S\to\infty}\big(\varepsilon_{K_0}\big)^{N_S}=0,\ \forall k\geq K_0$, which further means that there exists $k\geq K_0$ such that

$$\lim_{N_S\to\infty}\Pr\big\{\boldsymbol{\alpha}_{k+1}(n)\in\mathscr{L}_\varepsilon,\boldsymbol{\alpha}_k(n)\in\mathscr{L}_\varepsilon|\forall n\big\}=1.\quad(58)$$

This means that once a certain search particle hits the AOA $\mathscr{L}_\varepsilon$ around the global optimum solution, it is almost impossible to escape from this area, after sufficient iterations.

Furthermore, since $p(\mathbf{z}|\boldsymbol{\alpha}_R)$ is uniformly continuous, $\|\boldsymbol{\alpha}_R-\boldsymbol{\alpha}_R^\star\|_2\leq\delta$ if $\mathscr{P}^\star-p(\mathbf{z}|\boldsymbol{\alpha}_R)\leq\varepsilon$, given two upper bounded scalars $\delta>0$ and $\varepsilon>0$ that are properly defined. Thus, we have $\Pr\{\boldsymbol{\alpha}_{k+1}(n)\in\mathscr{L}_\varepsilon\}=\Pr\{\|\boldsymbol{\alpha}_{k+1}-\boldsymbol{\alpha}_R^\star\|_2\leq\delta\}$.

Therefore, combining the results in Eqs. (56) and (58), we can arrive at the conclusion that the PASS-based estimator in Eq. (30) satisfies $\lim\limits_{\substack{N_S\to\infty,\\k\to\infty}}\Pr\big\{\|\hat{\boldsymbol{\alpha}}_k(N_S)-\boldsymbol{\alpha}_R^\star\|_2\leq\delta\big\}=1,\ \forall\delta>0$. Then, Theorem 1 is proved.

APPENDIX D
THE PROOF OF THEOREM 2

Suppose the VLC-based SPAO system is unbiased. Then, the expectation of the maximum likelihood estimate (MLE) will approach the true value of the complete variable $\boldsymbol{\alpha}_R$, *i.e.*,

$$\mathbb{E}\big\{\boldsymbol{\alpha}_R^\star(|\Omega_R|)\big\}=\boldsymbol{\alpha}_R,\quad(59)$$

$$\kappa(\mathscr{L}_\varepsilon) = \iint\limits_{\substack{\boldsymbol{\alpha}_k(n)\in\mathscr{R},\\ \boldsymbol{\alpha}_k^\flat(n)\in\mathscr{L}_\varepsilon}} p\big(\boldsymbol{\alpha}_k^\flat(n)|\boldsymbol{\alpha}_k(n)\big)p\big(\boldsymbol{\alpha}_k(n)\big)\,\mathrm{d}\boldsymbol{\alpha}_k(n)\mathrm{d}\boldsymbol{\alpha}_k^\flat(n) \geq \underbrace{\iint\limits_{\substack{\boldsymbol{\alpha}_k(n)\in\mathscr{R},\\ \boldsymbol{\alpha}_k^\flat(n)\in\mathscr{L}_\varepsilon}} p\big(\boldsymbol{\alpha}_k(n)\big)\,\varrho\,\mathrm{d}\boldsymbol{\alpha}_k(n)\mathrm{d}\boldsymbol{\alpha}_k^\flat(n)}_{\iota(\mathscr{L}_\varepsilon)}. \tag{53}$$

where $\boldsymbol{\alpha}_R^\star(|\Omega_R|)$ is the MLE associated with measurement sample size $|\Omega_R|$, that is given in condition C3. Given a finite measurement size $|\Omega_R|$, there will be a certain error between $\boldsymbol{\alpha}_R^\star(|\Omega_R|)$ and its true value $\boldsymbol{\alpha}_R$. The covariance of this error is cast as

$$\begin{aligned}&\big(\boldsymbol{\alpha}_R^\star(|\Omega_R|)-\boldsymbol{\alpha}_R\big)\big(\boldsymbol{\alpha}_R^\star(|\Omega_R|)-\boldsymbol{\alpha}_R\big)^\top\\ &=\big(\boldsymbol{\mathcal{I}}(\boldsymbol{\alpha}_R)\big)^{-1}=\bigg(\sum_{m\in\Omega_R}\omega_m\mathbf{A}_m(\boldsymbol{\alpha}_R)\bigg)^{-1},\end{aligned} \tag{60}$$

where $\boldsymbol{\mathcal{I}}(\boldsymbol{\alpha}_R)$ denotes the Fisher information, and $\mathbf{A}_m(\boldsymbol{\alpha}_R)$ is the measurement resolution matrix, which are definite-positive and will be given by (34)–(44). In this case, we have that

$$\begin{aligned}&\lim_{|\Omega_R|\to\infty}\mathrm{trace}\Big(\big(\boldsymbol{\mathcal{I}}(\boldsymbol{\alpha}_R)\big)^{-1}\Big)\\ &=\lim_{|\Omega_R|\to\infty}\mathrm{trace}\bigg(\bigg(\sum_{m\in\Omega_R}\omega_m\mathbf{A}_m(\boldsymbol{\alpha}_R)\bigg)^{-1}\bigg)=0.\end{aligned} \tag{61}$$

This means that the gap between $\boldsymbol{\alpha}_R^\star\big(|\Omega_R|\big)$ and $\boldsymbol{\alpha}_R$ will be closed with sufficient measurement samples, $i.e.$,

$$\lim_{|\Omega_R|\to\infty}\boldsymbol{\alpha}_R^\star\big(|\Omega_R|\big)=\boldsymbol{\alpha}_R. \tag{62}$$

Based on Theorem 1, we know $\lim\limits_{\substack{N_S\to\infty,\\ k\to\infty}}\Pr\big\{\|\hat{\boldsymbol{\alpha}}_k(N_S)-\boldsymbol{\alpha}_R^\star\|_2\leq\varepsilon\big\}=1,\ \forall\varepsilon>0$. In consequence, we can arrive at the conclusion in Theorem 2.

APPENDIX E
DERIVATION OF EQ. (37), (38) AND (40)

The orientations $\mathbf{v}_m$ and $\mathbf{u}_R$ are unit vectors. Thus, given (6), the derivative vector $\nabla_{\mathbf{x}_R}h_m(\mathbf{x}_R,\mathbf{u}_R)$ can be formed as (63) (on the top of next page), where ρ_m and $\mathbf{e}_m$ are given in (44) and (2), respectively. Then, the measurement resolution factor $\boldsymbol{\Theta}_m(\mathbf{x}_R,\mathbf{x}_R)$ is finally derived as Eq. (37).

Given $\mathbf{y}_m$ in (42), where we consider $\mathbf{v}_m$ is a unit vector, the propagation function $h_m(\mathbf{x}_R,\mathbf{u}_R)$ in (6) can be rewritten as a compact function of $\mathbf{u}_R$ as follows,

$$h_m(\mathbf{x}_R,\mathbf{u}_R)=\Psi'_R\rho_m^{-2}\mathbf{y}_m^\top\frac{\mathbf{u}_R}{\|\mathbf{u}_R\|_2}. \tag{64}$$

Note that $\mathbf{y}_m$ and ρ_m are related to $\mathbf{x}_R$, rather than $\mathbf{u}_R$, as defined in Eqs. (42) and (44), respectively. Consequently, the derivative vector $\nabla_{\mathbf{u}_R}h_m(\mathbf{x}_R,\mathbf{u}_R)$ can be derived as

$$\nabla_{\mathbf{u}_R}h_m(\mathbf{x}_R,\mathbf{u}_R)=\Psi'_R\rho_m^{-2}\left(\frac{\|\mathbf{u}_R\|_2^2\,\mathbf{I}-\mathbf{u}_R\mathbf{u}_R^\top}{\|\mathbf{u}_R\|_2^3}\right)\mathbf{y}_m, \tag{65}$$

where $\mathbf{I}$ stands for the associated identity matrix.

Hence, based on Eq. (34), $\boldsymbol{\Theta}_m(\mathbf{x}_R,\mathbf{u}_R)$ are cast as Eq. (38), where we have considered that $\mathbf{u}_R$ is a unit vector.

Let $\mathbf{F}_m=\mathbf{y}_m\mathbf{y}_m^\top$, which can be further expressed as Eq. (43). Based on Eq. (65), considering that the orientation vector $\mathbf{u}_R$ is a unit vector, $\boldsymbol{\Theta}_m(\mathbf{u}_R,\mathbf{u}_R)$ can be derived as Eq. (40).

REFERENCES

[1] Y. S. Kuo, P. Pannuto, K. J. Hsiao, and P. Dutta, "Luxapose: Indoor positioning with mobile phones and visible light," *Proceedings of the 20th annual international conference on Mobile computing and networking*. ACM, 2014

[2] S. H. Yang, H. S. Kim, Y. H. Son and S. K. Han, "Three-Dimensional Visible Light Indoor Localization Using AOA and RSS With Multiple Optical Receivers," *Journal of Lightwave Technology*, Vol.32, No.14, 2014, pp.2480-2485.

[3] Y. Zhuang, L. Hua, L. Qi, J. Yang, P. Cao, Y. Cao, Y. Wu, J. Thompson, and H. Haas, "A Survey of Positioning Systems Using Visible LED Lights," to appear in *IEEE Communications Surveys & Tutorials*, 2018.

[4] A. Jovicic, J. Li and T. Richardson, "Visible Light Communication: Opportunities, Challenges and the Path to Market," *IEEE Communications Magazine,* Vol.51, No.12, 2013, pp.26-32.

[5] T. Komine and M. Nakagawa, "Fundamental analysis for visible-light communication system using LED lights," *IEEE Transactions on Consumer Electronics*, Vol.50, No.1, pp.100-107, Feb 2004.

[6] J. Armstrong, Y. A. Sekercioglu and A. Neild, "Vislbile Light Positioning: A Roadmap for international Standardization", *IEEE Communication Magzine*, Vol.51, No.12, 2013, pp.68-73.

[7] M. Yasir, S.-W. Ho, and B. N. Vellambi. "Indoor positioning system using visible light and accelerometer." *Journal of Lightwave Technology* 32.19 (2014): 3306-3316.

[8] C. Amini, A. Taherpour, T. Khattab and S. Gazor, "Theoretical accuracy analysis of indoor visible light communication positioning system based on time-of-arrival," *2016 IEEE Canadian Conference on Electrical and Computer Engineering (CCECE)*, Vancouver, BC, 2016, pp. 1-5.

[9] A. Sahin, Y. S. Eroglu, I. Guvenc, N. Pala, and M. Yuksel, "Accuracy of AOA-based and RSS-based 3D localization for visible light communications." *2015 IEEE 82nd. Vehicular Technology Conference (VTC Fall)* IEEE, 2015.

[10] M. Yasir, S.-W. Ho and B. N. Vellambi, "Indoor localization using visible light and accelerometer," *2013 IEEE Global Communications Conference (GLOBECOM)*, Atlanta, GA, 2013, pp.3341-3346.

[11] H. Kim, D. Kim, S. Yang, Y. Son, and S. Han, "An Indoor Visible Light Communication Positioning System Using a RF Carrier Allocation Technique," *J. Lightw. Technol.*, Vol.31, No.1, 2013, pp. 134-144.

[12] Y. S. Eroglu, I. Guvenc, N. Pala and M. Yuksel, "AOA-based localization and tracking in multi-element VLC systems," *2015 IEEE 16th Annual Wireless and Microwave Technology Conference (WAMICON)*, Cocoa Beach, FL, 2015, pp. 1-5.

[13] H. Sharifi, A. Kumar, F. Alam and K. M. Arif, "Indoor localization of mobile robot with visible light communication," *2016 12th IEEE/ASME International Conference on Mechatronic and Embedded Systems and Applications (MESA)*, Auckland, 2016, pp. 1-6.

[14] W. Zhang, M. S. Chowdhury, amd M. Kavehrad, "Asynchronous indoor positioning system based on visible light communications." *Optical Engineering*, Vol.53, No.4, 2014, pp.045105.1-045105.9,

[15] Z. Zhou, M. Kavehrad, and P. Deng, "Indoor Positioning Algorithm using Light-Emitting Diode Visible Light Communications," *Optical Engineering*, 51(8), 2012, 085009-1.

[16] L. Yin, X. Wu and H. Haas, "Indoor Visible Light Positioning with Angle Diversity Transmitter." *2015 IEEE 82nd Vehicular Technology Conference (VTC Fall)*. IEEE, 2015.

[17] G. B. Prince, and T. D. Little, "Latency constrained device positioning using a visible light communication two-phase received signal strength-angle of arrival algorithm." *2015 International Conference on Indoor Positioning and Indoor Navigation (IPIN),* IEEE, 2015, pp:1-7.

$$\nabla_{\mathbf{x}_R} h_m(\mathbf{x}_R, \mathbf{u}_R) = \Psi'_R \rho_m^{-3} \underbrace{\left[\mathbf{e}_m,\ \mathbf{u}_R,\ \mathbf{v}_m\right]}_{\mathbf{K}_m} \underbrace{\begin{bmatrix} -(r+3)(r+1)\left(\mathbf{e}_m^\top \mathbf{v}_m\right)^r \mathbf{e}_m^\top \mathbf{u}_R \\ (r+1)\left(\mathbf{e}_m^\top \mathbf{v}_m\right)^r \\ r(r+1)\left(\mathbf{e}_m^\top \mathbf{v}_m\right)^{r-1} \mathbf{e}_m^\top \mathbf{u}_R \end{bmatrix}}_{\mathbf{s}_m} = \Psi'_R \rho_m^{-3} \mathbf{K}_m \mathbf{s}_m. \tag{63}$$

[18] K. Qiu, F. Zhang and M. Liu, "Visible Light Communication-based indoor localization using Gaussian Process," *2015 IEEE/RSJ International Conference on Intelligent Robots and Systems (IROS)*, Hamburg, 2015, pp. 3125-3130

[19] J. Kennedy and R. Eberhart,"Particle swarm optimization," *Proc. IEEE Int. Conf. Neural Netwrork*, 1995, Vol.4, pp. 1942-1948.

[20] R. V. Kulkarni and G. K. Venayagamoorthy, "Particle Swarm Optimization in Wireless-Sensor Networks: A Brief Survey," *IEEE Transactions on Systems, Man, and Cybernetics, Part C (Applications and Reviews)*, Vol.41, No.2, pp.262-267, March 2011.

[21] Y. D. Valle, G. K. Venayagamoorthy, S. Mohagheghi, J. C. Hernandez and R. G. Harley, "Particle swarm optimization: basic concepts, variants and applications in power systems." *IEEE Trans. Evolutionary Computation*, Vol.12, No.2, 2008, pp.171-195.

[22] J. Kennedy, "Particle swarm optimization." *Encyclopedia of Machine Learning*. Springer US, 2010. pp.760-766.

[23] S. Sudibyo, M. N. Murat and N. Aziz, "Simulated annealing-Particle Swarm Optimization (SA-PSO): Particle distribution study and application in Neural Wiener-based NMPC," *2015 10th Asian Control Conference (ASCC)*, Kota Kinabalu, 2015, pp. 1-6.

[24] C.-R. Hwang. "Simulated annealing: theory and applications, "*Acta Applicandae Mathematicae*, Vol.12, No.1, 1988, pp.108-111.

[25] B. Suman, and P. Kumar. "A survey of simulated annealing as a tool for single and multiobjective optimization." *Journal of the operational research society*, Vol.57, No.10, 2006, pp.1143-1160.

[26] X. Zhang, J. Duan, Y. Fu and A. Shi, "Theoretical Accuracy Analysis of Indoor Visible Light Communication Positioning System Based on Received Signal Strength Indicator," *Journal of Lightwave Technology*, Vol.32, No.21, 2014, pp.4180-4186.

[27] H. Steendam, T. Q. Wang and J. Armstrong, "Cramer-Rao bound for indoor visible light positioning using an aperture-based angular-diversity receiver," *2016 IEEE International Conference on Communications (ICC)*, Kuala Lumpur, 2016, pp. 1-6.

[28] T. Q. Wang, Y. A. Sekercioglu, A. Neild and J. Armstrong, "Position Accuracy of Time-of-Arrival Based Ranging Using Visible Light With Application in Indoor Localization Systems," *Journal of Lightwave Technology*, Vol.31, No.20, pp.3302-3308, Oct.15, 2013.

[29] S. Rajagopal, R. D. Roberts, and S.-K. Lim. "IEEE 802.15. 7 visible light communication: modulation schemes and dimming support." *IEEE Communications Magazine,* 50(3):72-82, 2012.

[30] H. Elgala, R. Mesleh and H. Haas, "Indoor optical wireless communication: potential and state-of-the-art," *IEEE Communication Magazine*, Vol.49, No.9, 2011, pp.56-62.

[31] J. H. Y. Nah, R. Parthiban and M. H. Jaward, "Visible Light Communications localization using TDOA-based coherent heterodyne detection," *2013 IEEE 4th International Conference on Photonics (ICP)*, Melaka, 2013, pp. 247-249.

[32] J. Kahn and J. Barry, "Wireless Infrared Communications," *Proc. IEEE*, Vol.85, No.2, 1997, pp. 265-298.

[33] P. Luo, Z. Ghassemlooy, H. Le Minh, E. Bentley, A. Burton, and X. Tang, "Fundamental analysis of a car to car visible light communication system." *Communication Systems, Networks & Digital Signal Processing (CSNDSP), 2014 9th International Symposium on*. IEEE, 2014.

[34] X. Chen, and M. Jiang. "Adaptive statistical Bayesian MMSE channel estimation for visible light communication." *IEEE Transactions on Signal Processing* 65.5 (2017): 1287-1299.

[35] S. W. Ho, A. A. Saed, L. Lai, and C. W. Sung, "Coding and Bounds for Channel Estimation in Visible Light Communications and Positioning." *IEEE Journal on Selected Areas in Communications* 36.1 (2018): 34-44.

[36] J. Barry, J. Kahn, W. Krause, E. Lee, and D. Messerschmitt, "Simulation of Multipath Impulse Response for Indoor Wireless Optical Channels," *IEEE J. Select. Area Commun.*, Vol.11, No.3, 1993, pp. 367-379.

[37] J. Grubor, S. Randel, K. Langer, and J. W. Walewski, "Broadband Information Broadcasting Using LED-Based Interior Lighting," *IEEE J. Lightw. Technol.*, vol. 26, no. 24, pp. 3883-3892, Dec. 2008.

[38] Y. Wang, S. Videv, and H. Haas, "Dynamic Load Balancing with Handover in Hybrid Li-Fi and Wi-Fi Networks," *in Symposium on Personal Indoor and Mobile Radio Commun. (PIMRC)*, Sep. 2014, pp. 548-552.

[39] C. Chen, D. A. Basnayaka, X. Wu, and H. Haas, "Efficient Analytical Calculation of Non-Line-of-Sight Channel Impulse Response in Visible Light Communications." *Journal of Lightwave Technology* 36.9 (2018): 1666-1682.

[40] A. Al-Kinani, C. Wang, H. Haas and Y. Yang, "A geometry-based multiple bounce model for visible light communication channels." *Wireless Communications and Mobile Computing Conference (IWCMC), 2016 International*. IEEE, 2016.

[41] L. Zeng, D. O'Brien, H. Minh, G. Faulkner, K. Lee, D. Jung, Y. Oh, and E. T. Won, "High Data Rate Multiple Input Multiple Output (MIMO) Optical Wireless Communications Using White LED Lighting," *IEEE J. Sel. Areas Commun.*, Vol.27, No.9, 2009, pp. 1654-1662.

[42] B. Hajek, "Cooling Schedules for optimal annealing," *Mathematics of operation research*, 13.2 (1998): 311-329.

[43] C. J. P. Belisle, "Convergence Theorems For A Class Of Simulated Annealing Algorithms on $\mathbb{R}^d$," *Journal of Applied Probability*, 29.04 (1992): 885-895.

[44] B. Hajek. "A tutorial survey of theory and applications of simulated annealing." *Decision and Control, 1985 24th IEEE Conference on*. IEEE, 1985.

[45] B. Wang and D. M. Titterington, "Convergence properties of a general algorithm for calculating variational Bayesian estimates for a normal mixture model." *Bayesian Anal.*, Vol.1, No.3, 2006, pp.625-650

[46] T. Cover and J. Thomas, Elements of Information Theory, New York: John Wiley and Sons, Inc., 1991.

[47] S. N. Diggavi and T. M. Cover, Is maximum entropy noise the worst?, Proceedings of IEEE International Symposium on Information Theory, Ulm, 1997, pp.278.

[48] S. M. Kay, Fundamentals of Statistical Signal Processing, Vol. 2: Detection theory. *Prentice Hall PTR*, 1998.

[49] B. Zhou and Q. Chen, "On the Particle-Assisted Stochastic Search Mechanism in Wireless Cooperative Localization," *IEEE Transactions on Wireless Communications*, Vol.15, No.7, pp. 4765-4777, July 2016.

[50] B. Zhou, Q. Chen, H. Wymeersch, P. Xiao and L. Zhao, "Variational Inference-based Positioning with Nondeterministic Measurement Accuracies and Reference Location Errors," *IEEE Transactions on Mobile Computing.* Vol.16, No. 10, Oct, 2017, pp.2955-2969

[51] B. Zhou, Q. Chen, P. Xiao and L. Zhao, "On the Spatial Error Propagation Characteristics of Cooperative Localization in Wireless Networks," *IEEE Trans. Vehi. Tech.*, Vol.66, No.2, 2017, pp.1647-1658.

[52] S. Boyd, and Lieven Vandenberghe. Convex optimization. *Cambridge university press*, 2004.